Manuscript - with full author details

The G-patch activators Pfa1 and PINX1 exhibit different modes of interaction with the Prp43 RNA helicase

Saïda Mouffok*¶, Régine Capeyrou*, Kamila Belhabich-Baumas*, Clément Joret, Anthony K. Henras, Odile Humbert, and Yves Henry

Laboratoire de Biologie Moléculaire Eucaryote, Centre de Biologie Intégrative (CBI), Université de Toulouse, CNRS, UPS, 31000 Toulouse, France

CONTACT Yves Henry henry@ibcg.biotoul.fr, Odile Humbert odile.humbert@ibcg.biotoul.fr

*The authors wish it to be known that, in their opinion, the first three authors should be regarded as joint First Authors.

¶Present address: Laboratoire des Interactions Plantes Micro-organismes, Université de Toulouse, INRA, CNRS, 31326 Castanet-Tolosan Cedex, France

ABSTRACT

Prp43 is a DEAH-box RNA helicase involved in both splicing and ribosome biogenesis. Its activities are directly stimulated by several co-activators that share a G-patch domain. The substrates of Prp43, its mechanism of action and the modes of interaction with and activation by G-patch proteins have been only partially characterized. We investigated how Pfa1 and PINX1, two G-patch proteins involved in ribosome biogenesis, interact with Prp43. We demonstrate that a protruding loop connecting the β4 and β5 strands of Prp43 OB fold is crucial for the binding of the G-patch domain of Pfa1. However, neither this loop nor the entire OB fold of Prp43 are essential for PINX1 binding. We conclude that the binding modes of Pfa1 and PINX1 G-patches to Prp43 are different. Nevertheless, stimulation of the ATPase and helicase activities of Prp43 by both full-length Pfa1 and PINX1 requires the β4-β5 loop. Moreover, we show that disruption of this loop completely abrogates Prp43 activity during yeast ribosome biogenesis but does not prevent its integration within pre-ribosomal particles. We propose that the β4-β5 loop plays a crucial role in the transmission of conformational changes induced by binding of the G-patch to Prp43 active site and substrate RNA.

KEYWORDS

RNA helicase; ATPase; G-patch protein; OB fold; ribosome synthesis

Introduction

Proteins of the DExD/H family play crucial roles in all processes involving RNA-protein complexes, including translation, pre-mRNA splicing, mRNP transport, ribosome biogenesis and RNA decay [1-7]. They are thought to remodel RNA/RNA and/or RNA/protein interactions using nucleotide triphosphate (usually ATP) hydrolysis and are often referred to as RNA helicases because a subset can unwind base-paired RNA strands *in vitro* [8-10]. They exhibit a conserved core that contains the catalytic centre and often feature additional domains that may regulate their subcellular localization, target them to their specific substrates and/or modulate their activity [11]. DExD/H proteins can be involved in more than one process. One good example is the Prp43 helicase intervening in pre-mRNA splicing, ribosome biogenesis and probably other processes occurring in the cytoplasm. Prp43 belongs to the DEAH protein family, named from the amino acid sequence of conserved motif II within the core region. In addition to motif II, DEAH proteins share a similar domain organization. They feature an N-terminal extension specific to each protein, followed by the core region, a helix-turn-helix motif of the winged helix category, a ratchet domain constituted by a bundle of seven alpha helices and an OB fold close to the C-terminus adopting a five-stranded β-barrel topology [12-18]. The core region comprises two RecA-like domains, termed RecA1 and RecA2, involved in ATP binding and hydrolysis as well as nucleic acid binding.

During splicing, yeast Prp43 is required for the release of the U6 snRNA as well as the U2 and U5 snRNPs from the spliced out intron lariat allowing snRNA/snRNP recycling as well as lariat linearization and degradation [19-22]. Prp43 also performs a proofreading function during splicing by promoting the dissociation of stalled spliceosomes assembled on suboptimal or mutated pre-mRNAs [23, 24]. During ribosome biogenesis in yeast, Prp43 is required for the production of both small and large ribosomal subunits and interacts with most pre-ribosomal particles [25-27]. Finally, Prp43 could intervene in the remodelling of cytoplasmic RNPs (other than pre-ribosomal particles), that remain to be identified [28].

In yeast, Prp43 is assisted by several co-factors that directly bind to the enzyme, increase its ATPase activity and are required for the enzyme to function as a helicase, as demonstrated *in vitro* [28-31]. These co-factors all feature a G-patch domain, characterized by the presence of conserved glycine residues, hence the name [11, 32, 33]. In human also, several G-patch co-factors of human PRP43 (DHX15) have been identified

[34-39]. The yeast G-patch protein Ntr1 (also called Spp382) specifically activates Prp43 for intron lariat spliceosome (ILS) disassembly [22, 31, 40-42]. Two other yeast G-patch co-factors, Pfa1 (also known as Sqs1) and Gno1 (also called Pxr1) interact with Prp43 during ribosome biogenesis [29, 30, 43, 44]. Prp43 activation by Pfa1 seems required for efficient 20S pre-rRNA conversion into mature 18S rRNA by the Nob1 endonuclease within cytoplasmic pre-40S pre-ribosomal particles [30, 44]. Gno1 is required for normal accumulation of both small and large ribosomal subunits [43]. It is associated with early 90S pre-ribosomal particles as well as early pre-60S pre-ribosomal particles within which it could activate Prp43, thus driving further maturation of pre-60S and pre-40S particles [29, 45] (for reviews on ribosome biogenesis see [46, 47]).

The mechanism of action of Prp43, the conformational rearrangements it elicits and its direct molecular targets remain a subject of debate and intense research. Within the spliceosome, Prp43 targets the U2 snRNP/intron interaction and can be cross-linked to the pre-mRNA [41]. Prp43 may translocate on the pre-mRNA/intron and disrupt the interaction between U2 snRNA and the branch point region. Prp43 could also bind to U6 snRNA [48, 49]. Within pre-ribosomal particles, Prp43 likely has several substrates and roles. It is involved in the release of a subset of box C/D snoRNAs from 25S rRNA sequences [50]. Moreover, a major Prp43 interaction site was identified on 18S rRNA helix 44, close to 18S rRNA 3' end [50]. Apart from the disruption of some snoRNA/pre-rRNA interactions, the remodelling events driven by Prp43 in the 90S, pre-60S and pre-40S pre-ribosomal particles remain totally unknown.

Another key aspect being currently intensely investigated is the way DEAH proteins interact with and are activated by their G-patch partners. Until very recently, no detailed structural information on DEAH protein/G-patch interactions was available. In the cryo-EM structure of the yeast intron lariat spliceosome, the Ntr1 protein is present but the structure of its G-patch domain that mediates the interaction with Prp43 could not be resolved [48]. However, the crystal structures of helicase DHX15 bound to NKRF G-patch and of helicase Prp2 bound to Spp2 G-patch have just been published, providing for the first time detailed molecular insights into DEAH protein/G-patch interactions [39, 51] (see Fig. S1 for the structure of DHX15 bound to NKRF G-patch). Strikingly, the two G-patches interact with their partner helicase in an almost identical fashion, forming a flexible molecular brace across the helicase surface, which favours the adoption of a conformation with high RNA binding affinity.

We have studied in the present work how Prp43 interacts with and is activated by Pfa1 and PINX1, the human orthologue of yeast Gno1 (for a summary table of our main findings, see Table S1). Our results point to a crucial role of the protruding loop connecting the β4 and β5 strands of Prp43 OB fold in Prp43 activation by both Pfa1 and PINX1. Unexpectedly, however, our results also show that the G-patch containing domains of Pfa1 and PINX1 have different requirements for binding to Prp43. We propose that PINX1 interacts with Prp43 as NKRF or Spp2 do with their partner helicase [39, 51], while Pfa1 G-patch mode of binding to Prp43 appears significantly different.

Results

The loop connecting the β4 and β5 strands of Prp43 OB fold is crucial for the binding of the G-patch containing C-terminal domain of Pfa1

How Pfa1 interacts with and activates Prp43 has not been fully elucidated. In particular, the structure of the Prp43/Pfa1 complex has not been solved yet. We have previously shown that the domain encompassing the C-terminal 193 amino acids of Pfa1 containing the G-patch domain, hereafter termed Pfa1C-ter, can directly bind to Prp43 and stimulate its ATPase and helicase activities [30]. This C-terminal domain of Pfa1 is crucial for Prp43 stimulation since all truncated forms of Pfa1 that lack this domain are totally devoid of stimulatory potential. Pfa1C-ter fails to bind to a truncated form of Prp43 that lacks the C-terminal 110 amino acids, that we call Prp43ΔC-ter [17], suggesting that at least part of the binding site of Pfa1C-ter is located within the C-terminal 110 amino acids of Prp43. This region of Prp43 contains an OB fold beta barrel structure, followed by two C-terminal alpha helices (αC2 and αC3, Fig. 1A). To identify which of these structural elements are crucial for Pfa1C-ter binding, we performed immunoprecipitation experiments with Pfa1C-ter and truncated/mutated versions of Prp43 (see Fig. S2 for Coomassie and Western analyses of purified proteins used in this work). We tested a form of Prp43 lacking the C-terminal alpha helix αC3 (see Fig. 1A-B), termed Prp43ΔαC3, while unfortunately, the effect of removing the two C-terminal alpha helices of Prp43 could not be assessed since we failed to express the corresponding protein in *E. coli*. We also assessed the binding to Prp43 variants featuring nested deletions and amino-acid substitutions within loops of the OB fold connecting the β strands 1 and 2 (Prp43mL1-2, Fig. 1A) or 4 and 5 (Prp43mL4-5, Fig. 1A) [17]. We reasoned that since these loops are protruding and solvent exposed in the Prp43 structure [17], they are prime candidates for constituting direct contact sites for G-patch domains. The mutations introduced in these loops were designed to both shorten them and remove long positively charged or polar amino acid side chains. To control for the proper folding of these Prp43 variants, we also tested their ability to interact with the N-terminal domain of Pfa1 encompassing amino acids 1 to 202, hereafter termed Pfa1N-ter, which can independently bind to Prp43ΔC-ter [17]. These immunoprecipitation experiments were performed with purified recombinant proteins and polyclonal anti-Prp43 antibodies. As shown in Fig. 1B, lane 3, deletion of the C-terminal alpha helix αC3 does not prevent binding of Prp43ΔαC3 to Pfa1C-ter, ruling out the

possibility that this helix constitutes a crucial Prp43 interaction surface for Pfa1C-ter. A substantial amount of Pfa1C-ter is recovered in the supernatant (Fig. 1.B, lane 4), as observed when the immunoprecipitation is performed with wild-type Prp43 [30] (see also Fig. 3B), reflecting the lower affinity of Pfa1C-ter for Prp43 compared to full length Pfa1. Prp43mL1-2 could not interact with Pfa1C-ter (Fig. 1C, lane 3). However, Prp43mL1-2 also failed to interact with the N-terminal domain of Pfa1 (Pfa1N-ter, Fig. 1C, lane 5), rendering interpretation of the data difficult. Indeed, it is not obvious to explain why Prp43mL1-2 cannot interact with Pfa1N-ter while Prp43ΔC-ter can do so [17], without invoking substantial folding defects. In contrast, Prp43mL4-5 did not bind to Pfa1C-ter but could interact with both Pfa1 and Pfa1N-ter, arguing that Prp43mL4-5 is properly folded (Fig. 1D, lanes 1, 3 and 5). Note that the failure to detect Pfa1C-ter in the IP lanes 3 of Fig. 1C and 1D and Pfa1N-ter in the IP lane 5 of Fig. 1C indicates that these truncated proteins do not interact on their own with the antibody-coated sepharose beads, as previously demonstrated by us [30].

On the basis of the above results, we predicted that Pfa1 or Pfa1C-ter should not stimulate the biochemical activities of Prp43mL4-5. This was first tested by performing ATPase assays using Prp43 (Fig. 2A), Prp43ΔC-ter (Fig. 2B) or Prp43mL4-5 (Fig. 2C), either alone or together with Pfa1 or Pfa1C-ter. As previously published, Prp43 ATPase activity is strongly stimulated by Pfa1 and to a lesser extent by Pfa1C-ter (Fig. 2A, see also [30]). In contrast, Prp43ΔC-ter ATPase activity fails to be stimulated by either Pfa1 or Pfa1C-ter (Fig. 2B, see also [17]). As observed for Prp43ΔC-ter, the ATPase activity of Prp43mL4-5 is not stimulated by Pfa1C-ter (Fig. 2C), and exhibits only a very slight increase in the presence of full length Pfa1 (Fig. 2C). We next analysed the effects of the removal of Prp43 C-terminal domain or mutation of the β4-β5 loop on its helicase activity driven by Pfa1- or Pfa1C-ter (Fig. 2D and S3A). Strikingly, whereas Pfa1 and Pfa1C-ter confer robust helicase activity to wild-type Prp43 (Fig. 2D, lanes 5 and 11 and Fig. S3A, lane 5), they hardly or completely fail to stimulate the helicase activity of Prp43ΔC-ter or Prp43mL4-5 (Fig. 2D, lanes 6, 7, 12, 13 and Fig. S3A, lane 7).

We conclude that the integrity of Prp43 β4-β5 loop is crucial for the interaction with the C-terminal domain of Pfa1 and hence for the activation of Prp43 by Pfa1.

The N-terminal alpha helix of Prp43 is not required for binding to the N-terminal domain of Pfa1

Prp43 contains an N-terminal extension comprising three alpha helices that is not found in other DEAH RNA helicases (Fig. 3A). This domain might function as an interaction surface for specific Prp43 partners. We hypothesized that this N-terminal extension of Prp43 might constitute the binding site for the N-terminal domain of Pfa1, Pfa1N-ter (Fig. 3A), which, as previously stated, can bind on its own to Prp43ΔC-ter [17]. *In vivo*, the N-terminal domain of Pfa1 seems important for pre-rRNA processing at sites A1 and A2. Indeed, expression of a Pfa1 truncated variant lacking this N-terminal domain in *Δpfa1* cells leads to the disappearance of the 32S and 27SA2 pre-rRNAs, reduced levels of 20S pre-rRNA and increased accumulation of 23S pre-rRNA [30] (for a cartoon of pre-rRNA processing in *S. cerevisiae*, see [52]). To investigate whether the N-terminal domain of Prp43 is required for binding to the N-terminal domain of Pfa1, we performed pull down assays using Pfa1N-ter and truncated versions of Prp43 lacking the first alpha helix and linker sequence (Prp43ΔαN1, Fig. 3A) or all three N-terminal alpha helices (Prp43ΔαN1-N3, Fig. 3A). To control for the proper folding of these Prp43 truncated variants, we assessed their ability to interact with Pfa1C-ter. Since our anti-Prp43 polyclonal serum was produced with Prp43 N-terminal peptides, it could not be used to precipitate the N-terminally truncated Prp43 variants. Hence GST-tagged truncated Prp43 proteins, or wild-type Prp43 as control, were used to allow their pull down with glutathione sepharose. GST-tagged wild-type Prp43 could interact with both Pfa1C-ter (Fig. 3B, lane 1) and Pfa1N-ter (Fig. 3B, lane 3). Removal of the first alpha helix and linker sequence of Prp43 did not prevent the interaction with Pfa1C-ter (Fig. 3C, lane 1) or Pfa1N-ter (Fig. 3C, lane 3). However, the amount of unbound Pfa1N-ter recovered in the supernatant fraction increased compared to the immunoprecipitation performed with wild-type Prp43 (compare lanes 3 and 4 of Fig. 3B and 3C), suggesting that lack of the first alpha helix and linker sequence of Prp43 slightly reduces its affinity for Pfa1N-ter. Removal of all three N-terminal alpha helices impaired Prp43 binding to Pfa1N-ter (Fig. 3D, lanes 3 and 4). However, this truncated version of Prp43 also failed to interact with the C-terminal domain of Pfa1 (Fig. 3D, lanes 1 and 2), preventing us from drawing any firm conclusion from these results. The failure to detect Pfa1C-ter in the IP of Fig. 3D, lane 1 and Pfa1N-ter in the IP of Fig. 3D, lane 3 indicates that these proteins do not interact with glutathione sepharose on their

own. We conclude that the first N-terminal alpha helix and linker of Prp43 are not essential for binding of the N-terminal domain of Pfa1 but may strengthen the interaction.

The Prp43 OB fold domain is not essential for the binding of PINX1 to Prp43 but necessary for full Prp43 activation by PINX1

Prp43 interacts with two G-patch proteins involved in ribosome biogenesis, Pfa1 and Gno1. We have shown that PINX1, the Gno1 human orthologue that can functionally replace Gno1 in yeast, can directly bind to yeast Prp43 and activate its ATPase [29] and helicase activities (Fig. 2D, lane 8 and Fig. S3A). Substitutions of conserved amino acids within the G-patch domain of PINX1 prevent the interaction with Prp43, indicating that PINX1 binds to Prp43 via the G-patch [29]. The Prp43 domain required for PINX1 binding remains unknown. To test whether the C-terminal OB fold-containing domain of Prp43 is required for PINX1 binding, we performed immunoprecipitation experiments using purified PINX1 and either Prp43ΔC-ter or Prp43mL4-5. Contrary to our expectations, and in sharp contrast to the C-terminal domain of Pfa1, PINX1 could bind to both Prp43ΔC-ter and Prp43mL4-5 (Fig. 4A, lanes 1 and 3). Note that on its own, PINX1 does not bind to antibody-coated sepharose beads (Fig. 4A, lane 5; see also [29]). Nevertheless, removal of the C-terminal domain of Prp43, but not the mL4-5 mutation, reduces the affinity of PINX1 for Prp43, as shown by the detection of unbound PINX1 in the supernatant lane 2 of Fig. 4A, but not in the supernatant lane 4 of Fig. 4A (Prp43mL4-5) or in the supernatant lane 2 of Fig. 4B (wild-type Prp43, see also [29]).

To assess the impact of an N-terminal truncation on the ability of Prp43 to interact with PINX1, we performed immunoprecipitation experiments using PINX1 and Prp43ΔαN1 or Prp43 as control. PINX1 could interact with both Prp43 (Fig. 4B, lane 1) and Prp43ΔαN1 (Fig. 4B, lane 3). We conclude that neither the first alpha helix of the N-terminal domain of Prp43 nor the OB fold and surrounding alpha helices of the C-terminal domain of Prp43 are essential for PINX1 binding.

Although the C-terminal domain of Prp43 is not required for PINX1 binding, it might nevertheless be important for Prp43 activation by PINX1. To investigate this hypothesis, we first performed ATPase assays, which demonstrate that Prp43ΔC-ter ATPase activity is only very weakly stimulated by addition of PINX1 (Fig. 5). Prp43mL4-5 ATPase activity is increased by PINX1 to a greater extent, but far less than wild-type Prp43 (Fig. 5). We next set up helicase assays using Prp43, Prp43ΔC-ter or Prp43mL4-5 and PINX1 (Fig. 2D and Fig.

S3A). As stated above, we could show for the first time that PINX1, like Pfa1, can confer strong helicase activity to Prp43 (Fig. 2D, lanes 5 and 8, Fig. S3A, lanes 5 and 6). In contrast, PINX1 cannot confer helicase activity to Prp43ΔC-ter or Prp43mL4-5 (Fig. 2D, lanes 9 and 10 and Fig. S3A, lane 8). We conclude that the C-terminal domain of Prp43 is not essential for PINX1 binding, unlike what is found for Pfa1C-ter, but necessary for full enzyme activation by PINX1.

Mutually exclusive interactions of Pfa1 and PINX1 with Prp43 in vitro

The fact that Prp43 C-terminal domain is necessary for binding of Pfa1C-ter but dispensable for PINX1 association leaves open the possibility that Pfa1 and PINX1 can bind simultaneously to Prp43. However, we failed to detect in yeast extracts an interaction between Pfa1 and Gno1 (the orthologue of PINX1) [29], arguing that formation of a Gno1/Pfa1/Prp43 trimeric complex is unlikely to occur. To assess whether formation of a PINX1/Pfa1/Prp43 complex can form *in vitro*, we incubated together purified recombinant GST-PINX1, Pfa1 and Prp43 and we proceeded to either pull-down experiments with glutathione sepharose (Fig. 6A) or immunoprecipitation experiments with anti-PINX1 antibodies (Fig. 6B). In both cases, a fraction of Prp43 was co-precipitated with PINX1 (Fig. 6A and B, lanes 1), confirming formation of a PINX1-Prp43 complex. Pfa1 was found in the supernatant fractions only (Fig. 6A and B, lanes 2) together with some Prp43, likely corresponding to the Prp43 fraction bound to Pfa1 prior to pull-down. The failure to detect co-precipitation of Pfa1 with PINX1 in the presence of Prp43 argues that Prp43 can interact with only one G-patch co-factor at a time.

Integrity of Prp43 C-terminal domain is crucial for ribosome biogenesis

The finding that Prp43mL4-5 displays no helicase activity *in vitro* in the presence of PINX1 suggests that the β4-β5 loop is crucial for Prp43 function in ribosome biogenesis *in vivo*. To test this hypothesis, we expressed Prp43mL4-5 from a centromeric vector in *GAL::prp43* cells in which the chromosomal copy of *PRP43* can be switched off by shifting cells from galactose to glucose-containing medium. We also included N- and C-terminal truncated mutants of Prp43 (Prp43ΔαN1, Prp43ΔαN1-N2, Prp43ΔαN1-N3, Prp43ΔαC2-C3, Prp43ΔC-ter) in the same analysis. All mutant proteins can be produced in *GAL::prp43* cells depleted of

endogenous Prp43, with the exception of Prp43ΔαN1 which was not studied further (Fig. 7A and data not shown). We also reproducibly observed a lower accumulation of Prp43ΔC-ter compared to wild-type Prp43p (Fig. 7A), maybe due to its lack of integration within pre-ribosomal particles (see below) that may increase its turnover. Neither Prp43ΔC-ter nor Prp43mL4-5 can support growth of *GAL::prp43* cells in glucose-containing medium, while under the same conditions, cells expressing Prp43ΔαC2-C3 display a severe growth defect (Fig. S4). In contrast, cells expressing Prp43ΔαN1-N2 or Prp43ΔαN1-N3 grow in glucose-containing medium as well as cells expressing wild-type Prp43. We conclude that the N-terminal domain of Prp43 does not exert an essential function, in accordance with a previous analysis [21]. This finding is also consistent with the results of a double-hybrid analysis showing that Prp43 N-terminal domain is not necessary for interaction with G-patch proteins required for normal growth, Gno1 and Ntr1 [53]. Contrary to the N-terminal domain, the C-terminal domain and the β4-β5 loop are essential for Prp43 function.

Northern analysis indicates that pre-rRNA processing in cells expressing Prp43ΔC-ter and Prp43mL4-5 is impaired to the same extent as in cells depleted of endogenous Prp43 transformed with the empty vector (Fig. 7B and S5A, lanes 1, 3 and 7 and Fig. S5B). These cells display an accumulation of 35S pre-rRNA and a depletion of all downstream pre-rRNA processing intermediates (32S, 27SA2, 27SB, 20S pre-rRNAs), i.e. the typical pattern of Prp43-depleted cells [26]. This is illustrated by a strong and highly statistically significant decrease in 27SA2/35S, (27SA2 + 27SB)/35S and 20S/35S ratios compared to those of the wild-type control (Fig. S5B and Table S2). We conclude that disruption of the β4-β5 loop completely abrogates Prp43 function in ribosome biogenesis. Cells expressing Prp43ΔαC2-C3 also display a strong pre-rRNA processing defect (Fig. 7B and S5A, lane 6, Fig. S5B and Table S2), underscoring the importance of the alpha helices adjacent to Prp43 OB fold. However, contrary to cells transformed with the empty vector or expressing Prp43ΔC-ter and Prp43mL4-5, cells expressing Prp43ΔαC2-C3 contain some 32S pre-rRNA and display a statistically significant two fold higher 27SA2/35S ratio (Fig. S5B and Table S2), indicating that early pre-rRNA processing events are slightly less impaired. This is consistent with the fact that *GAL::prp43* cells expressing Prp43ΔαC2-C3 are able to grow, albeit very slowly (Fig. S4). In contrast, cells expressing Prp43ΔαN1-N2 or Prp43ΔαN1-N3 do not exhibit obvious pre-rRNA processing defects (Fig. 7B and S5A, lanes 4 and 5, Fig. S5B and Table S2), confirming that the N-terminal domain of Prp43 is largely dispensable, at least under our experimental conditions.

To ascertain that the β4-β5 loop disruption prevents Prp43 activation per se *in vivo*, but does not impair its interaction with pre-ribosomal particles, the ability of Prp43mL4-5 to interact with pre-rRNAs was assessed by immunoprecipitation experiments. This analysis had to be performed under conditions of endogenous Prp43 depletion, since overproduction of endogenous Prp43 in galactose-containing medium reduces incorporation within pre-ribosomal particles of wild-type Prp43 expressed from plasmid-encoded transcripts (data not shown). Northern analysis shows that the 35S pre-rRNA is co-precipitated with ProtA-tagged Prp43mL4-5 as efficiently as with ProtA-tagged wild-type Prp43 (Fig. 7D, lanes 6 and 8), indicating that it is indeed incorporated within the initial 90S pre-ribosomal particles. Interestingly, in contrast, 35S pre-rRNA is not detectably co-precipitated with Prp43ΔC-ter over background (Fig. 7D, lane 7), even though the Prp43ΔC-ter protein itself is precipitated to the same extent as Prp43mL4-5 (Fig. 7C). We conclude that the C-terminal domain of Prp43 is required for its efficient incorporation and/or retention within initial pre-ribosomal particles.

Discussion

The multifunctional DEAH RNA helicase Prp43 plays crucial roles in different cellular processes, including pre-mRNA splicing and ribosome biogenesis, and at distinct steps of these two processes. Moreover, it associates with different G-patch co-factors that are crucial activators of Prp43 enzymatic activities, at least *in vitro* [11, 33]. The direct RNA/RNP targets of Prp43, its mechanism of action and its mode of activation by G-patch proteins are major issues that are not fully resolved. In particular, how the G-patch protein Pfa1 interacts with and activates Prp43 remains to be clarified. We previously showed that the C-terminal domain of Pfa1 containing the G-patch constitutes a Prp43 interaction and activation domain [30]. A truncated version of Pfa1, Pfa1(1-565), that lacks the C-terminal G-patch containing domain is able to bind to Prp43 via the N-terminal region of Pfa1 but is unable to activate Prp43 [30]. In a subsequent study, we initiated the search for the domain(s) of Prp43 that contact the G-patch containing C-terminal domain of Pfa1. We showed that the C-terminal OB fold-containing domain of Prp43 is crucial for the binding of the G-patch containing domain of Pfa1 (Pfa1C-ter) [17]. In the present study, we further show that the C-terminal alpha helix αC3 of Prp43 is not necessary for the binding of Pfa1C-ter (for a summary of the properties of Prp43 mutants, see Table S1). More importantly, we demonstrate that the integrity of the loop connecting the β4 and β5 strands of Prp43 OB fold is crucial for the binding of Pfa1C-ter. Thus this loop may constitute a direct and crucial contact point for the C-terminal domain of Pfa1. Alternatively or in addition, the integrity of the β4-β5 loop may be necessary for the correct folding of a nearby Prp43 domain necessary for Pfa1 G-patch binding (see below). The binding sites(s) for PINX1 on Prp43 have not been identified thus far and we expected them to be located within the C-terminal OB fold containing domain of Prp43. This expectation was reinforced by our failure to detect formation of a Pfa1/Prp43/PINX1 complex *in vitro,* strongly suggesting that binding of Pfa1 and Gno1/PINX1 to Prp43 are mutually exclusive. This exclusivity notion was also strengthened by the finding that isolated G-patch domains of Pfa1, Gno1 or Cmg1, a recently-described cytoplasmic activator of Prp43, compete for the binding of the G-patch domain of Ntr1 to Prp43 [28]. However, we found that the C-terminal domain of Prp43 was not essential for the binding of PINX1, consistent with the recent observation that Gno1 can interact in a double hybrid assay with a truncated form of Prp43 lacking most of the C-terminal domain [53]. Our finding could not be explained by the presence of two functionally independent

Prp43 binding sites within PINX1 as is the case for Pfa1 since the integrity of the G-patch domain is essential for full length PINX1 binding to Prp43 [29]. While this manuscript was in preparation, the crystal structures of helicase DHX15 bound to the G-patch of NKRF and of splicing helicase Prp2 bound to the G-patch of Spp2 were reported [39, 51]. In both structures, the G-patch binds its partner helicase in a similar way, forming a flexible molecular brace across the helicase surface. It interacts with the helicase mostly via two anchor points. The N-terminal alpha helix of the G-patch packs on the long alpha helix of the winged helix domain while the C-terminal loop stacks into a hydrophobic pocket at the top of the RecA2 domain. Studer and collaborators [39] propose that the G-patch increases the activity of the helicase by restricting the mobility of the RecA2 domain relative to the rest of the structure and favouring the adoption of a conformation with high RNA binding affinity. Strikingly, no specific contacts between the G-patch and the OB fold domain of the helicase were reported. The finding that the entire OB fold domain of Prp43 is dispensable for PINX1 binding argues that PINX1 interacts with Prp43 in a similar fashion to NKRF and Spp2 with DHX15 and Prp2, respectively. The dependency of Pfa1C-ter on the OB fold and the integrity of the β4-β5 loop for binding to Prp43 indicates that its mode of interaction is significantly different. Strikingly, in both the DHX15/NKRF G-patch and Prp2/Spp2 G-patch structures, the C-terminal part of the G-patch is found in the vicinity of the equivalent of the β4-β5 loop of the helicase (see Fig. S1). In particular, T742 and T743 of the β4-β5 loop of DHX15 OB fold and H586 and K587 of NKRF G-patch are close (Fig. S1). The C-terminal part of Pfa1 G-patch may make a direct and crucial contact with the β4-β5 loop. Alternatively, β4-β5 loop mutations may impact folding of the top of the RecA2 domain or its β hairpin in such a way that Pfa1C-ter binding, but not that of PINX1, is prevented. We note however that the Prp43mL4-5 protein in which the β4-β5 loop has been disrupted is not grossly misfolded since it exhibits normal basal ATPase activity and is able to bind to PINX1 and to the N-terminal domain of Pfa1.

Interestingly, Pfa1 and PINX1 have different effects on Prp43 helicase activity *in vitro*. In complex with PINX1, Prp43 displays a helicase activity with a strict 3'-5' specificity (Fig. S3C, compare lanes 4 and 8), as described for a majority of helicases [54, 55]. In contrast, the Prp43/Pfa1 complex is capable of unwinding a duplex nucleic acid substrate with a 5' overhang that could not be unwound by the Prp43/PINX1 complex, albeit with lower efficiency compared with the equivalent substrate with a 3' overhang (Fig. S3C, compare lanes 3 and 7). This ability to open a duplex with a 5' overhang may be imparted by an

interaction between Pfa1 and the OB fold and more specifically the region encompassing the β4-β5 loop, that could modify the position of the RNA substrate within the RNA-binding channel. The fact that Pfa1 possesses an N-terminal Prp43 interaction domain may also contribute to the differences in helicase activity characteristics. The *in vivo* functional consequences of the biochemical differences between the two complexes remain to be investigated. They may have evolved to better deal with different RNA substrates. Indeed, one of the specific functions of the Prp43/Gno1 complex may be to disrupt a subset of box C/D snoRNA/pre-rRNA associations within 90S particles [45], while one or several major specific targets of the Prp43/Pfa1 complex are likely intramolecular RNA structures of the 20S pre-rRNA in pre-40S particles, with which Pfa1 displays a prominent association [26]. In particular, Prp43 interacts with sequences that form helix h44 of mature 18S rRNA [50] and the region encompassing the connected helices h28, h44 and h45 undergoes conformational rearrangements right until the end of pre-40S particle maturation [56]. The Prp43/Pfa1 complex is believed to contribute to some of these rearrangements [44, 56] and the ability of this complex to unwind RNA duplexes with 5' or 3' single-stranded extremities may be required at this stage.

Since PINX1 can still bind to Prp43mL4-5 but fails to fully stimulate the ATPase activity of Prp43mL4-5 (in absence of RNA) compared to its effect on wild-type Prp43, we conclude that somehow the integrity of the β4-β5 loop is necessary for the catalytic centre to adopt the correct structure following G-patch binding. In addition, we have previously shown that the ATPase activity of Prp43mL4-5 is less stimulated by RNA than wild-type Prp43 [17]. Thus the OB fold region encompassing the β4-β5 loop might also provide contact points for RNA. This is supported by the finding of the β4-β5 loop in close proximity to RNA in a Prp43/poly-uracil crystal structure [13]. The crucial role of the β4-β5 loop is underscored by the fact that Prp43mL4-5 cannot sustain the viability of Prp43-depleted cells. This is due, at least in part, to the inability of Prp43mL4-5 to support normal pre-rRNA processing. Since Prp43mL4-5 is integrated within the initial 90S pre-ribosomal particles and yet its expression leads to the same pre-rRNA processing defects as lack of Prp43, we conclude that Prp43mL4-5 activity as such is largely, if not fully impaired during ribosome biogenesis. Results from our *in vitro* helicase assays suggest that it is the failure of Prp43mL4-5-Pfa1 and Prp43mL4-5-Gno1/PINX1 complexes to function as helicases *in vivo* that is the main reason for the observed ribosome biogenesis defects. Interestingly, while our results show that the integrity of the β4-β5 loop is not required for the integration of Prp43 within 90S pre-ribosomal

particles, they also indicate that Prp43 C-terminal domain encompassing the OB fold and C-terminal alpha helices is essential for this integration.

Materials and methods

E. coli and yeast strains, media and plasmids

E. coli strains directing expression of Prp43-HIS, GST-PINX1-HIS, GST-Prp43-HIS, GST-Prp43ΔαN1-HIS, GST-Prp43ΔαN1-N3-HIS, Prp43ΔαC3-HIS, Pfa1-HIS, Pfa1C-ter-HIS, Pfa1N-ter-HIS were obtained by transforming *E. coli* BL21 λDE3 with plasmids pSL18 [30], pRC43 [29], pFM15, pFM16, pFM17, pFM19, pSL20 [30], pSL53bis [30], pSL55 [30], respectively.

pFM15 was obtained by inserting into BamHI digested pGEX-4T1 a BglII digested *PRP43-HIS* PCR cassette obtained by amplifying the *PRP43* ORF using oligonucleotides 5'GST Prp43 (5'GGGGGAGATCTATGGGTTCCAAAAGAAGATTCTCGTCCGAACACCCGGATCCAGTTG3') and Prp43inpsO2 (5'GGGGGAGATCTTCAGTGGTGGTGGTGGTGGTGTTTCTTGGAGTGCTTACTCTTCTTTT3'). pFM16 was obtained by inserting into BamHI digested pGEX-4T1 a BglII digested *PRP43(59-767)-HIS* PCR cassette obtained by amplifying the *PRP43* ORF using oligonucleotides 5'GST Prp43(59-767) (5'GGGGGAGATCTTCAGCAGAAGAGGCCCAAAAACTTGAAGATGGAAAAATAAATC3') and Prp43inpsO2. pFM17 was obtained by inserting into BamHI digested pGEX-4T1 a BglII digested *PRP43(92-767)-HIS* PCR cassette obtained by amplifying the *PRP43* ORF using oligonucleotides 5'GST Prp43(92-767) (5'GGGGGAGATCTGAATTGCCAGTACATGCCCAGAGAGATGAGTTTTTAAAAC3') and Prp43inpsO2. pFM19 was obtained by inserting into XbaI/XhoI digested pSCodon1 a SpeI/XhoI digested *PRP43(1-723)-HIS* PCR cassette obtained by amplifying the *PRP43* ORF using oligonucleotides

Prp43 inps O1 (5'GGGGGGACTAGTTTTAAGAAGGAGATATACATATGGGTTCCAAAAGAAGATTCTCGTCC3') and 3'Prp43(1-723) (5'CCCCC*CTCGAG*TCAGTGGTGGTGGTGGTGGTGAGGCGCTATTTCAATCAGCCATTCGGGCCTGACCGAGGTCAC3').

An *E. coli* strain directing expression of Prp43ΔC-ter-HIS was obtained by transforming *E. coli* SE1 with plasmid pMFX [17]. Plasmids encoding Prp43mL1-2-HIS (combined K663A, R664G mutations and deletion of residues 665–668) and Prp43mL4-5-HIS (combined T702G, S703G mutations and K704 deletion) were derived from pSL18 by GenScript Corporation (Piscataway, NJ) [17] and transformed into strain SE1.

A *GAL::HA-prp43* strain was obtained by transforming into a *Saccharomyces cerevisiae* strain (*his3-Δ200 leu2-Δ1 trp1-Δ63 ura3-52)* a KanMX6-GAL1-10-3HA PCR cassette flanked by *PRP43* promoter sequences obtained by PCR amplification performed with plasmid pFA6a-kanMX6-PGAL1-3HA [57] as template and oligonucleotides OHA424 (5'ATTCAATTGTAATATTTAACACGTTTACGGGGATGCGATTGAGTAACGATGAA TTCGAGCTCGTTTAAAC3') and OHA426 (5'GTCTCAACTGGATCCGGGTGTTCGGACGAGAATCTTCTTTTGGAACCCATGCAC TGAGCAGCGTAATCTG3'). To obtain *S. cerevisiae* strains expressing Prp43ΔC-ter, Prp43ΔαN1-N2, Prp43ΔαN1-N3, Prp43ΔαC2-C3, Prp43mL4-5, or wild-type Prp43 fused two IgG binding domains (ZZ) of *S. aureus* protein A, the *GAL::HA-prp43* strain was transformed with centromeric plasmids derived from pHA113 [58], termed pFM14, pFM10, pFM11, pFM13, pFM18 and pFM7. To construct pFM7, the *PRP43* ORF was amplified with oligonucleotides 5'SCPRP43 (5'GGGGGAGATCTAATGGGTTCCAAAAGAAGATTCTCGTCCGAAC3') and 3'SCPRP43 (5'GGGGGAGATCTAATTTCTTGGAGTGCTTACTCTTCTTTTTGTTTTTACC3') and pSL18 as template, the resulting PCR product was digested with BglII and inserted into BamHI cut pHA113. To construct pFM10 or pFM11, the *PRP43* ORF was amplified with pSL18 as template, oligonucleotides 5'SCPRP43(80-767) (5'GGGGGAGATCTTACACCAAAATATGTTGATATCCTGAAAATTAG3') or 5'SCPRP43(92-767) (5'GGGGGAGATCTAGAATTGCCAGTACATGCCCAGAGAGATGAG3'), respectively, and 3'SCPRP43, the resulting PCR product was digested with BglII and inserted into BamHI cut pHA113. To construct pFM13 or pFM14, the *PRP43* ORF was amplified with pSL18 as template, oligonucleotides 5'SCPRP43 and 3'SCPRP43(1-713) (5'GGGGGAGATCTAAGACCGAGGTCACAGTTCTTATGTAGTTCTTCGATG3') or 3'SCPRP43(1-657) (5'GGGGGAGATCTAAGAAAAACCCAGACGCAAGAGCCTTTCTGATGTTG3'), the

resulting PCR product was digested with BglII and inserted into BamHI cut pHA113. To construct pFM18, the 1958 bp AgeI/AflII fragment within *PRP43* ORF was digested from pSL18-Prp43mL4-5-HIS (see above) and used to replace the corresponding fragment in pFM7. Strains have been grown in YP (1% yeast extract, 2% peptone) supplemented with 2 % galactose or 2 % glucose or in YNB (1.7 g/L) supplemented with ammonium sulphate (5 g/L) and 2 % galactose or 2 % glucose.

Protein purification

Recombinant protein purifications from transformed *E. coli* BL21 λDE3 bacteria were performed as described in [29].

Immunoprecipitations with recombinant proteins

They were performed as described in [29], except that anti-PINX1 antibodies (ab99112, Abcam) were used in some immunoprecipitations.

Immunoprecipitations using yeast extracts

Immunoprecipitations using yeast extracts were performed using IgG-sepharose as described in [59] except that 200 mM KCl was used in the buffer for extract preparation and washing steps. Northern and western blot experiments to analyse input and immunoprecipitated samples were performed as in [59].

GST-Pull down experiments

A total of 2 µg of each recombinant purified protein were mixed in the indicated combinations and incubated with 50 µl of Glutathione beads (Thermo Scientific) in 500 µl IP buffer (25 mM Tris-HCl (pH 8.0), 300 mM KCl, 5 mM $MgCl_2$, 10% glycerol, 0.1% NP-40, 0.5 mM DTT) with gentle shaking for 1 h at 4°C. The supernatant was collected and proteins precipitated with TCA. Beads were washed four times with 1 ml IP buffer and proteins retained on the beads were eluted with 50 µl SDS-PAGE loading buffer (100 mM Tris-HCl (pH 6.8), 4% SDS, 20% glycerol, 200 mM DTT, 0.04% bromophenol blue). Proteins were analysed by Western blotting using His mAb HRP conjugate (Clontech).

ATPase assays

The ATPase activity of the proteins (0.1 μM) was measured in a 5 μl reaction volume containing 25 mM Tris-acetate (pH 8.0), 10 mM $Mg(CH_3COO)_2$, 0.2 mM DTT, 100 μg/ml BSA (Sigma) and 0.6 μCi/μl [α-^{32}P] ATP and unlabeled ATP at 100 μM. The reaction mixtures were incubated at 30°C for 0, 5, 10, 30 and 60 min, stopped on ice and 1 μl from each sample was analyzed by thin layer chromatography on PEI-Cellulose plates (Merck) using 0.75 M KH_2PO_4 as migration buffer. The plates were dried and radioactivity was quantified on a Fuji BAS 3000 Phosphorimager.

Helicase assays

They were performed as described in [30].

Acknowledgements

We thank members of our team for helpful discussions.

Disclosure of potential conflicts of interest

The authors report no conflict of interest.

Funding

This work was supported by the CNRS; Université Paul Sabatier; Ligue Contre le Cancer (équipe labellisée to Y.H.); Agence Nationale de la Recherche (ANR-2010-BLAN-1224 to Y.H.); Ministère de l'Enseignement Supérieur et de la Recherche (to S.M.).

References

1. Bleichert, F. and S.J. Baserga, *The long unwinding road of RNA helicases.* Mol Cell, 2007. **27**(3): p. 339-52.
2. Bourgeois, C.F., F. Mortreux, and D. Auboeuf, *The multiple functions of RNA helicases as drivers and regulators of gene expression.* Nat Rev Mol Cell Biol, 2016. **17**(7): p. 426-38.
3. De, I., J. Schmitzova, and V. Pena, *The organization and contribution of helicases to RNA splicing.* Wiley Interdiscip Rev RNA, 2016. **7**(2): p. 259-74.
4. Khemici, V. and P. Linder, *RNA helicases in RNA decay.* Biochem Soc Trans, 2018. **46**(1): p. 163-172.
5. Martin, R., et al., *DExD/H-box RNA helicases in ribosome biogenesis.* RNA Biol, 2013. **10**(1): p. 4-18.
6. Rodriguez-Galan, O., J.J. Garcia-Gomez, and J. de la Cruz, *Yeast and human RNA helicases involved in ribosome biogenesis: current status and perspectives.* Biochim Biophys Acta, 2013. **1829**(8): p. 775-90.
7. Liu, Y.C. and S.C. Cheng, *Functional roles of DExD/H-box RNA helicases in Pre-mRNA splicing.* J Biomed Sci, 2015. **22**: p. 54.
8. Gilman, B., P. Tijerina, and R. Russell, *Distinct RNA-unwinding mechanisms of DEAD-box and DEAH-box RNA helicase proteins in remodeling structured RNAs and RNPs.* Biochem Soc Trans, 2017. **45**(6): p. 1313-1321.
9. Jankowsky, E., *RNA helicases at work: binding and rearranging.* Trends Biochem Sci, 2011. **36**(1): p. 19-29.
10. Jarmoskaite, I. and R. Russell, *RNA helicase proteins as chaperones and remodelers.* Annu Rev Biochem, 2014. **83**: p. 697-725.
11. Sloan, K.E. and M.T. Bohnsack, *Unravelling the Mechanisms of RNA Helicase Regulation.* Trends Biochem Sci, 2018. **43**(4): p. 237-250.
12. He, Y., G.R. Andersen, and K.H. Nielsen, *Structural basis for the function of DEAH helicases.* EMBO Rep, 2010. **11**(3): p. 180-6.
13. He, Y., et al., *Structure of the DEAH/RHA ATPase Prp43p bound to RNA implicates a pair of hairpins and motif Va in translocation along RNA.* RNA, 2017. **23**(7): p. 1110-1124.
14. Kudlinzki, D., et al., *Structural analysis of the C-terminal domain of the spliceosomal helicase Prp22.* Biol Chem, 2012. **393**(10): p. 1131-40.
15. Tauchert, M.J., et al., *Structural and functional analysis of the RNA helicase Prp43 from the thermophilic eukaryote Chaetomium thermophilum.* Acta Crystallogr F Struct Biol Commun, 2016. **72**(Pt 2): p. 112-20.
16. Tauchert, M.J., et al., *Structural insights into the mechanism of the DEAH-box RNA helicase Prp43.* Elife, 2017. **6**.
17. Walbott, H., et al., *Prp43p contains a processive helicase structural architecture with a specific regulatory domain.* EMBO J, 2010. **29**(13): p. 2194-204.
18. Hamann, F., M. Enders, and R. Ficner, *Structural basis for RNA translocation by DEAH-box ATPases.* Nucleic Acids Res, 2019. **47**(8): p. 4349-4362.
19. Arenas, J.E. and J.N. Abelson, *Prp43: An RNA helicase-like factor involved in spliceosome disassembly.* Proc Natl Acad Sci U S A, 1997. **94**(22): p. 11798-802.
20. Fourmann, J.B., et al., *Dissection of the factor requirements for spliceosome disassembly and the elucidation of its dissociation products using a purified splicing system.* Genes Dev, 2013. **27**(4): p. 413-28.

21. Martin, A., S. Schneider, and B. Schwer, *Prp43 is an essential RNA-dependent ATPase required for release of lariat-intron from the spliceosome.* J Biol Chem, 2002. **277**(20): p. 17743-50.
22. Tsai, R.T., et al., *Spliceosome disassembly catalyzed by Prp43 and its associated components Ntr1 and Ntr2.* Genes Dev, 2005. **19**(24): p. 2991-3003.
23. Mayas, R.M., et al., *Spliceosome discards intermediates via the DEAH box ATPase Prp43p.* Proc Natl Acad Sci U S A, 2010. **107**(22): p. 10020-5.
24. Semlow, D.R. and J.P. Staley, *Staying on message: ensuring fidelity in pre-mRNA splicing.* Trends Biochem Sci, 2012. **37**(7): p. 263-73.
25. Combs, D.J., et al., *Prp43p is a DEAH-box spliceosome disassembly factor essential for ribosome biogenesis.* Mol Cell Biol, 2006. **26**(2): p. 523-34.
26. Lebaron, S., et al., *The splicing ATPase prp43p is a component of multiple preribosomal particles.* Mol Cell Biol, 2005. **25**(21): p. 9269-82.
27. Leeds, N.B., et al., *The splicing factor Prp43p, a DEAH box ATPase, functions in ribosome biogenesis.* Mol Cell Biol, 2006. **26**(2): p. 513-22.
28. Heininger, A.U., et al., *Protein cofactor competition regulates the action of a multifunctional RNA helicase in different pathways.* RNA Biol, 2016. **13**(3): p. 320-30.
29. Chen, Y.L., et al., *The telomerase inhibitor Gno1p/PINX1 activates the helicase Prp43p during ribosome biogenesis.* Nucleic Acids Res, 2014. **42**(11): p. 7330-45.
30. Lebaron, S., et al., *The ATPase and helicase activities of Prp43p are stimulated by the G-patch protein Pfa1p during yeast ribosome biogenesis.* EMBO J, 2009. **28**(24): p. 3808-19.
31. Tanaka, N., A. Aronova, and B. Schwer, *Ntr1 activates the Prp43 helicase to trigger release of lariat-intron from the spliceosome.* Genes Dev, 2007. **21**(18): p. 2312-25.
32. Aravind, L. and E.V. Koonin, *G-patch: a new conserved domain in eukaryotic RNA-processing proteins and type D retroviral polyproteins.* Trends Biochem Sci, 1999. **24**(9): p. 342-4.
33. Robert-Paganin, J., S. Rety, and N. Leulliot, *Regulation of DEAH/RHA helicases by G-patch proteins.* Biomed Res Int, 2015. **2015**: p. 931857.
34. Chen, Z., et al., *Identification of a 35S U4/U6.U5 tri-small nuclear ribonucleoprotein (tri-snRNP) complex intermediate in spliceosome assembly.* J Biol Chem, 2017. **292**(44): p. 18113-18128.
35. Lin, M.L., et al., *Involvement of G-patch domain containing 2 overexpression in breast carcinogenesis.* Cancer Sci, 2009. **100**(8): p. 1443-50.
36. Memet, I., et al., *The G-patch protein NF-kappaB-repressing factor mediates the recruitment of the exonuclease XRN2 and activation of the RNA helicase DHX15 in human ribosome biogenesis.* Nucleic Acids Res, 2017. **45**(9): p. 5359-5374.
37. Niu, Z., et al., *Tumor suppressor RBM5 directly interacts with the DExD/H-box protein DHX15 and stimulates its helicase activity.* FEBS Lett, 2012. **586**(7): p. 977-83.
38. Wen, X., S. Tannukit, and M.L. Paine, *TFIP11 interacts with mDEAH9, an RNA helicase involved in spliceosome disassembly.* Int J Mol Sci, 2008. **9**(11): p. 2105-13.
39. Studer, M.K., et al., *Structural basis for DEAH-helicase activation by G-patch proteins.* Proc Natl Acad Sci U S A, 2020.
40. Boon, K.L., et al., *Yeast ntr1/spp382 mediates prp43 function in postspliceosomes.* Mol Cell Biol, 2006. **26**(16): p. 6016-23.
41. Fourmann, J.B., et al., *The target of the DEAH-box NTP triphosphatase Prp43 in Saccharomyces cerevisiae spliceosomes is the U2 snRNP-intron interaction.* Elife, 2016. **5**.

42. Fourmann, J.B., et al., *Regulation of Prp43-mediated disassembly of spliceosomes by its cofactors Ntr1 and Ntr2.* Nucleic Acids Res, 2017. **45**(7): p. 4068-4080.
43. Guglielmi, B. and M. Werner, *The yeast homolog of human PinX1 is involved in rRNA and small nucleolar RNA maturation, not in telomere elongation inhibition.* J Biol Chem, 2002. **277**(38): p. 35712-9.
44. Pertschy, B., et al., *RNA helicase Prp43 and its co-factor Pfa1 promote 20 to 18 S rRNA processing catalyzed by the endonuclease Nob1.* J Biol Chem, 2009. **284**(50): p. 35079-91.
45. Robert-Paganin, J., et al., *Functional link between DEAH/RHA helicase Prp43 activation and ATP base binding.* Nucleic Acids Res, 2017. **45**(3): p. 1539-1552.
46. Henras, A.K., et al., *An overview of pre-ribosomal RNA processing in eukaryotes.* Wiley Interdiscip Rev RNA, 2015. **6**(2): p. 225-42.
47. Kressler, D., E. Hurt, and J. Bassler, *A Puzzle of Life: Crafting Ribosomal Subunits.* Trends Biochem Sci, 2017. **42**(8): p. 640-654.
48. Wan, R., et al., *Structure of an Intron Lariat Spliceosome from Saccharomyces cerevisiae.* Cell, 2017. **171**(1): p. 120-132 e12.
49. Toroney, R., K.H. Nielsen, and J.P. Staley, *Termination of pre-mRNA splicing requires that the ATPase and RNA unwindase Prp43p acts on the catalytic snRNA U6.* Genes Dev, 2019. **33**(21-22): p. 1555-1574.
50. Bohnsack, M.T., et al., *Prp43 bound at different sites on the pre-rRNA performs distinct functions in ribosome synthesis.* Mol Cell, 2009. **36**(4): p. 583-92.
51. Hamann, F., et al., *Structural analysis of the intrinsically disordered splicing factor Spp2 and its binding to the DEAH-box ATPase Prp2.* Proc Natl Acad Sci U S A, 2020. **117**(6): p. 2948-2956.
52. Henras, A.K., et al., *The post-transcriptional steps of eukaryotic ribosome biogenesis.* Cell Mol Life Sci, 2008. **65**(15): p. 2334-59.
53. Banerjee, D., P.M. McDaniel, and B.C. Rymond, *Limited portability of G-patch domains in regulators of the Prp43 RNA helicase required for pre-mRNA splicing and ribosomal RNA maturation in Saccharomyces cerevisiae.* Genetics, 2015. **200**(1): p. 135-47.
54. Pyle, A.M., *Translocation and unwinding mechanisms of RNA and DNA helicases.* Annu Rev Biophys, 2008. **37**: p. 317-36.
55. Singleton, M.R., M.S. Dillingham, and D.B. Wigley, *Structure and mechanism of helicases and nucleic acid translocases.* Annu Rev Biochem, 2007. **76**: p. 23-50.
56. Cerezo, E., et al., *Maturation of pre-40S particles in yeast and humans.* Wiley Interdiscip Rev RNA, 2019. **10**(1): p. e1516.
57. Longtine, M.S., et al., *Additional modules for versatile and economical PCR-based gene deletion and modification in Saccharomyces cerevisiae.* Yeast, 1998. **14**(10): p. 953-61.
58. Henras, A., et al., *Accumulation of H/ACA snoRNPs depends on the integrity of the conserved central domain of the RNA-binding protein Nhp2p.* Nucleic Acids Res, 2001. **29**(13): p. 2733-46.
59. Joret, C., et al., *The Npa1p complex chaperones the assembly of the earliest eukaryotic large ribosomal subunit precursor.* PLoS Genet, 2018. **14**(8): p. e1007597.

Figure legends

Figure 1. Effects of deletions and/or amino acid substitutions within Prp43 C-terminal domain on Pfa1C-ter binding. (A) Top: Schematics of Pfa1 and Prp43 domain organization and mutants used in IPs. Bottom: Structure of Prp43 OB fold and terminal alpha helices. Mutations in loops connecting strands β1 and β2 (mL1-2) and strands β4 and β5 (mL4-5) are highlighted. Mutation mL1-2 corresponds to K663A, R664G amino acid substitutions and deletion of residues 665 to 668. Mutation mL4-5 corresponds to T702G, S703G amino acid substitutions and deletion of K704. The structure was drawn using the data deposited in the protein data base (PDB) under the code 2xau [17]. (B-D) Purified HIS-tagged mutant versions of Prp43, namely Prp43ΔαC3 (B), Prp43mL1-2 (C) or Prp43mL4-5 (D), were mixed with either purified HIS-tagged Pfa1, Pfa1C-ter or Pfa1N-ter prior to immunoprecipitation using anti-Prp43 antibodies. Proteins from the supernatants were then TCA precipitated. Proteins present in the pellets (lanes IP) and in the supernatants (lanes Sup) were separated by SDS-PAGE, transferred to nitrocellulose membranes and analysed by Western using HRP-coupled anti-histidine antibodies.

Figure 2. Prp43mL4-5 is unable to be stimulated by Pfa1 or Pfa1C-ter. (A-C) Time course of [α-^{32}P]-ATP hydrolysis by HIS-tagged purified Prp43 (A), Prp43ΔC-ter (B) or Prp43mL4-5 (C) either alone or incubated with HIS-tagged purified Pfa1 or Pfa1C-ter. The percentage of hydrolysed ATP is plotted with respect to time (in minutes). The values plotted are means of three independent experiments. The standard error of the mean (sem) is shown by brackets. (D) Helicase assays. A RNA duplex formed by hybridisation of a short radiolabelled RNA to a longer unlabelled RNA was incubated with the indicated purified proteins (Prp43-HIS or derivatives, Pfa1-HIS or Pfa1C-ter-HIS, GST-PINX1-HIS). The reaction mixes were then treated with proteinase K, nucleic acids were separated by acrylamide gel electrophoresis and detected by autoradiography. Lane 1: free single-stranded labelled RNA.

Figure 3. The N-terminal 58 amino acids of Prp43 are dispensable for its binding to the N-terminal domain of Pfa1. (A) Schematics of Pfa1 and Prp43 domain organization and mutants used in IPs. (B-D) GST-Prp43-HIS (B), GST-Prp43ΔαN1-HIS (C) or GST-Prp43ΔαN1-N3-HIS (D) were mixed with either Pfa1C-ter-HIS (lanes 1 and 2) or Pfa1N-ter-HIS (lanes 3 and 4) prior to pull-down of GST-tagged proteins with glutathione sepharose. Pellet (IP) and

supernatant fractions (Sup) were then processed as described in the legend of Fig. 1. HIS-tagged proteins were detected by Western using HRP-coupled anti-histidine antibodies.

Figure 4. The C-terminal domain and N-terminal alpha helix of Prp43 are not essential for its interaction with GST-PINX1-HIS. (A) Analysis of the interactions between GST-PINX1-HIS and either Prp43ΔC-ter-HIS or Prp43mL4-5-HIS. Purified recombinant GST-PINX1-HIS was mixed with either Prp43ΔC-ter-HIS (lanes 1 and 2) or Prp43mL4-5-HIS (lanes 3 and 4) and precipitation was carried out with anti-Prp43 antibodies. A control precipitation was also performed with GST-PINX1-HIS (lanes 5 and 6) alone. Pellet (IP) and supernatant (Sup) fractions were processed as described in the legend of Fig. 1. HIS-tagged proteins were detected by Western using HRP-coupled anti-histidine antibodies. (B) Analysis of the interactions between GST-PINX1-HIS and Prp43ΔαN1. Purified recombinant GST-PINX1-HIS was mixed with either GST-Prp43-HIS (lanes 1 and 2) or GST-Prp43ΔαN1-HIS (lanes 3 and 4) prior to immunoprecipitation with anti-PINX1 antibodies. Sample processing and Western analysis was carried out as described in (A).

Figure 5. The integrity of the C-terminal domain of Prp43 is required for the full activation of Prp43 by GST-PINX1-HIS. Time course of [α-^{32}P]-ATP hydrolysis by Prp43-HIS, Prp43ΔC-ter-HIS or Prp43mL4-5-HIS either alone or incubated with GST-PINX1-HIS. The values plotted are means of three independent experiments. The standard error of the mean (sem) is shown by brackets.

Figure 6. Interactions of GST-PINX1-HIS and Pfa1-HIS with Prp43-HIS are mutually exclusive *in vitro*. (A) Pull down experiments. GST-PINX1-HIS, Pfa1-HIS and Prp43-HIS (lanes 1 and 2) or GST-PINX1-HIS and Pfa1-HIS (lanes 3 and 4), were mixed prior to pull down of GST-PINX1-HIS and associated proteins with glutathione sepharose. Pellet (IP) and supernatant fractions (Sup) were then processed as described in the legend of Fig. 1. HIS-tagged proteins were detected by Western using HRP-coupled anti-histidine antibodies. (B) As in (A), except that immunoprecipitations were carried out with anti-PINX1 antibodies.

Figure 7. Integrity of Prp43 C-terminal domain is essential for ribosome biogenesis. (A) Western analysis of accumulation of ProtA-tagged wild-type (WT) or Prp43 variants in *GAL::prp43* cells grown 13 hours in glucose-containing minimal medium. Empty: cells

transformed with empty parental vector. Prp43 proteins were detected using rabbit PAP. Pgk1, detected using specific antibodies, was used as loading control. (B) Northern analysis of pre-rRNA accumulation in *GAL::prp43* cells depleted of endogenous Prp43 and expressing ProtA-tagged wild-type (WT) or the indicated Prp43 variants. Names of the various pre-rRNAs detected using anti-sense oligonucleotide probes are indicated on the right. (C) Western analysis of ProtA-tagged wild-type (WT), Prp43ΔC-ter (ΔC-ter) or Prp43mL4-5 (mL4-5) precipitation. Precipitation experiments were carried out with IgG-sepharose and extracts of *GAL::prp43* cells transformed with plasmids directing expression of the above-listed proteins or the empty vector and grown 13 hours in glucose-containing minimal medium. Input: aliquots of input extracts; IPs: precipitated samples. Prp43 proteins were detected using rabbit PAP. (D) Corresponding Northern analysis to assess 35S pre-rRNA co-precipitation. The 35S pre-rRNA immunoprecipitation efficiency relative to wild-type (arbitrarily set at 1) assessed by phosphorimager scanning of the Northern blot is indicated below each IP lane.

Supplementary Figure Legends

Figure S1. Structure of DHX15 in complex with the NKRF G-patch (protein database code number: 6SH7). The blown up section shows the loop connecting the beta strands 4 and 5 (L4-5) of DHX15 OB fold (red) and the C-terminus of NKRF G-patch (black thread). The electron cloud surfaces of amino acids T742 and T743 of DHX15 L4-5 and of H586 and K587 of NKRF G-patch are depicted. The structure was drawn using the Molsoft ICM-browser.

Figure S2. Analysis of purified proteins used in this work by Coomassie staining (A, 1 µg each) and Western blot using HRP-coupled anti-histidine antibodies (B, 200 ng each).

Figure S3. Pfa1 and PINX1 can both confer helicase activity to Prp43 with different specificities. (A) Helicase assays with wild-type Prp43 or Prp43mL4-5 mutant. A RNA fragment hybridised to a radiolabelled DNA oligonucleotide was incubated with the indicated purified proteins (Prp43-HIS, Prp43mL4-5-HIS, Pfa1-HIS, GST-PINX1-HIS) or no protein as control (lane 2). The reaction mixes were then treated with proteinase K, nucleic acids were separated by acrylamide gel electrophoresis and detected by autoradiography. Lane 1: free labelled oligonucleotide. (B) Helicase assays with a duplex RNA substrate featuring a 3'

single-stranded overhang, Prp43-HIS (100 nM) and increasing concentrations of either Pfa1-HIS or GST-PINX1-HIS (0, 25, 50, 75, 100, 150, 200 nM) performed as indicated in (A). Lanes 1: free single-stranded labelled RNA. Right: plot of the percentage of unwinding with respect to G-patch protein concentration. (C) Helicase assays with Prp43-HIS and either Pfa1-HIS or GST-PINX1-HIS (50 nM). Same as in (A), except that duplex nucleic acid substrates with either a 3' single-stranded overhang (lanes 2-4) or a 5' single-stranded overhang (lanes 6-8) were used. Lanes 1 and 5: free labelled oligonucleotide.

Figure S4. Prp43mL4-5 fails to support growth. *GAL::prp43* cells were transformed with centromeric vectors directing expression of ProtA-tagged wild-type Prp43, Prp43ΔC-ter, Prp43ΔαN1-N3, Prp43ΔαN1-N2, Prp43ΔαC2-C3, Prp43mL4-5 or the parental empty vector (empty). Transformed strains were streaked on galactose- (left) or glucose- (right) containing medium.

Figure S5. Northern analysis of the effects of Prp43 mutations on pre-rRNA processing. (A) Northern analysis performed as described in the legend of Fig. 7B. (B) Histograms of the means of 27SA2/35S, (27SA2 + 27SB)/35S and 20S/35S pre-rRNA ratios from three independent biological replicates of the Northern blot shown in (A). These ratios were obtained by phosphorimager scanning of Northern blots and quantification of pre-rRNA species using the Multi Gauge software. Standard errors of the mean (sem) computed using the Excel software are shown. A statistical analysis of these ratios is presented in Table S2.

Table S1. Summary of the properties of Prp43 and G-patch proteins and their derivatives used in this work. Empty spaces indicate that the corresponding analyses have not been performed.

Table S2. Statistical analysis of rRNA processing intermediate ratios.

Dr Renee Schroeder
Editor-in-Chief
RNA Biology

Dear Dr Schroeder,

Please find below a point-by-point answer to the reviewers' comments. The corresponding changes to the manuscript text are highlighted in yellow.

To answer the concerns of the reviewers, we have added the following new figures and tables:

- Figure S1: Published NKRF G-patch/DHX15 complex with the position of the loop connecting the beta strands 4 and 5 highlighted.

- Figure S2: Coomassie-stained gel and Western analysis of all purified proteins used in pull-down/immunoprecipitation, ATPase and helicase assays.

- Figures S3: Helicase assays: A. Replicates of the helicase assays shown in Figure 2D. B and C: panels A and B of former Figure S1.

- Figure S4: Former Figure S2.

- Figure S5: Replicate of Northern of Figure 7B and quantitative analysis of pre-rRNA processing differences.

- Table S1: Summary of the properties of Prp43 and G-patch proteins and their derivatives used in this work.

- Table S2: Statistical analysis of rRNA processing intermediate ratios.

Novel data have also been added to Figures 2, 5 and 7 as detailed below.

We hope that the manuscript will now be judged suitable for publication in *RNA Biology*.

Sincerely,

Yves Henry and Odile Humbert

Reviewer 1:

However, the authors should also include biological replicates of their data as appropriate. While the authors fulfill the one-replicate standard-of-proof common in the field for immunoprecipitation experiments, the rigor of this manuscript would be greatly strengthened by showing additional biological replicates for the ATPase, helicase, and pre-rRNA processing assays. Additionally, quantification of the pre-rRNA processing intermediate ratios and of the pulldown ratio in Figure 7D would further bolster the manuscript's conclusions.

Major comments:

1. *The authors should include biological replicates of the ATPase (Figure 2A-C, Figure 5), helicase assays (Figure 2D), or pre-rRNA processing northerns (Figure 7B).*

The standard errors of the mean (sem) based on three replicates are now indicated on the ATPase assay plots (Figure 2A-C, Figure 5). Helicase assays have been performed with additional mutants, namely Prp43 mutant Prp43ΔC-ter and Pfa1 mutant Pfa1C-ter (new Figure 2D). Additional helicase assays are presented in new Figure S3A. Replicates of pre-rRNA processing Northerns are presented in new Figure S5, quantifications of various pre-rRNA ratios have been performed and subjected to ANOVA statistical tests (see below, Figure S5 and Table S2).

2. *Figure 7B: To quantitatively communicate defects observed in pre-rRNA processing, the authors should graph the northern blot pre-rRNA processing results using Ratio Analysis of Multiple Precursor (RAMP) quantification for all replicates [Wang, M., Anikin, L. & Pestov, D.G. Two orthogonal cleavages separate subunit RNAs in mouse ribosome biogenesis. Nucleic Acids Res 42, 11180-11191 (2014)]. Appropriate ANOVA testing can then be used to illustrate statistically-significant differences in processing intermediate levels.*

We have performed ratio analyses taking into account the major pre-rRNA intermediates (35S, 27SA2, 27SB, 20S pre-rRNAs) using the Northern data from three biological replicates (new Figure S5). ANOVA has been performed with these ratios (Table S2), which indicates strongly statistically significant differences between the wild-type control and a subset of mutants.

3. *Figure 7D: The authors should quantify the pulldown ratio to clarify the result. It is difficult to compare WT and mL4-5 by eye because of unequal loading.*

The immunoprecipitation efficiency of 35S pre-rRNA in mutants relative to wild-type has been quantified and is now indicated below each IP lane (Figure 7D).

Minor comments:

4. *Figure 2D: Correct PINXI to PINX1.*

This has been corrected throughout.

5. *p. 6: I don't think [30] contains the cited Pfa1N-ter and Prp43ΔC-ter experiment. However, this is shown in [17] (Figure 6, lane 11). The citation should be corrected.*

This citation has been corrected.

6. *p. 11: Correct phrasing in sentence "In contrast, cells expressing Prp43ΔN1-N2 or Prp43ΔN1-N3 grow in glucose-containing medium as cells expressing wild-type Prp43." to "grow in glucose-containing medium as well as cells expressing wild-type Prp43."*

This sentence has been corrected.

7. *All immunoprecipitation figures: I recommend noting which antibody was used for pulldown in each immunoprecipitation figure panel. The antibodies used in Figure 6 were not obvious, although they are in the legend. It would make the story easier to follow.*

The antibodies or type of sepharose used have been indicated in each immunoprecipitation/pull-down figure panel.

Reviewer 2:

1. *While an assay of the ATPase activity is a useful start, it would be equally useful to assess helicase activity, at least with a subset of the most important mutants.*

As indicated above in the answer to point 1 of reviewer 1, helicase assays have been performed with additional mutants, namely Prp43 mutant Prp43ΔC-ter and Pfa1 mutant Pfa1C-ter (new Figure 2D).

2. *The inputs of the in vitro pulldowns must be shown in order to assess them properly. Without those one cannot draw any strong conclusions from the pulldowns.*

All our pull-down/immunoprecipitation experiments have been performed with the same amounts of purified recombinant proteins, not with cell extracts. Moreover, we have shown the unbound material (supernatant) for each pull-down/immunoprecipitation, hence from the data presented it is clear what proportion of input protein is precipitated. We have now included a Coomassie stained gel of all the purified proteins used and a corresponding Western blot (new Figure S2).

3. *Full length Pfa1 and PINX1 both bind to Prp43mL4-5. It is only when they use the two Pfa1 fragments that deficiencies in binding to Prp43mL4-5 are uncovered. A similar experiment with PINX1 was not done. Thus, the conclusion that Pfa1 and PINX1 interact with Prp43 differently is not supported by the data. The authors should compare the binding of the G patch domain of Pfa1 with the G patch domain of PINX1 on binding of Prp43ΔC-ter or Prp43mL4-5.*

Our previously published data indicate that Pfa1 deleted of its G patch can still interact with Prp43. In sharp contrast, point mutations within the G patch of full length PINX1 prevent its binding to full length Prp43 both *in vitro* and in yeast cells (Chen et al., Nucleic Acids Res., 2014). Hence, contrary to Pfa1 G patch, the G patch of PINX1 is essential for its binding to Prp43. Thus our finding that PINX1 interacts with Prp43ΔC-ter or Prp43mL4-5 indicates that its G-patch does not require Prp43 C-terminal domain for binding.

4. *I am assuming that the authors were trying to make a mutant that separates the Gno1 and Pfa1-dependent functions of Prp43. While they found a mutant that is deficient only in Pfa1 binding, this mutant turned out to be useless because it is required for Gno1/PINX1-dependent Prp43 activation. Why did the authors not carry out a more comprehensive analysis of Prp43 truncations and mutants for some deficient in Gno1/PINX1 binding? At the very least, one would expect them to test all the ones tested for Pfa1. But to be honest, in order for this to be a meaningful contribution for the field, I think one should have a separation mutant.*

While we agree with the reviewer that obtaining a separation mutant would have been very interesting, we do think that providing evidence for the crucial role of the OB fold domain and in particular its beta 4- beta 5 loop is an important contribution to the field.

5. *The manuscript is extremely hard to follow. I would suggest the authors lead with a Figure of the published G-patch/DEAH-helicase complex, to better illustrate the rationale for these experiments. A summary of the roles of the different elements in Prp43, PINX1 and Pfa1 studied in here for binding and activation by the G-patch proteins would also be helpful.*

We have included a figure of the published NKRF G-patch/DHX15 complex and highlighted the position of the loop connecting the beta strands 4 and 5 (new Figure S1). We also added a table (Table S1) summarising the roles of the domains of Prp43 and G-patch proteins studied here.

Figure 1

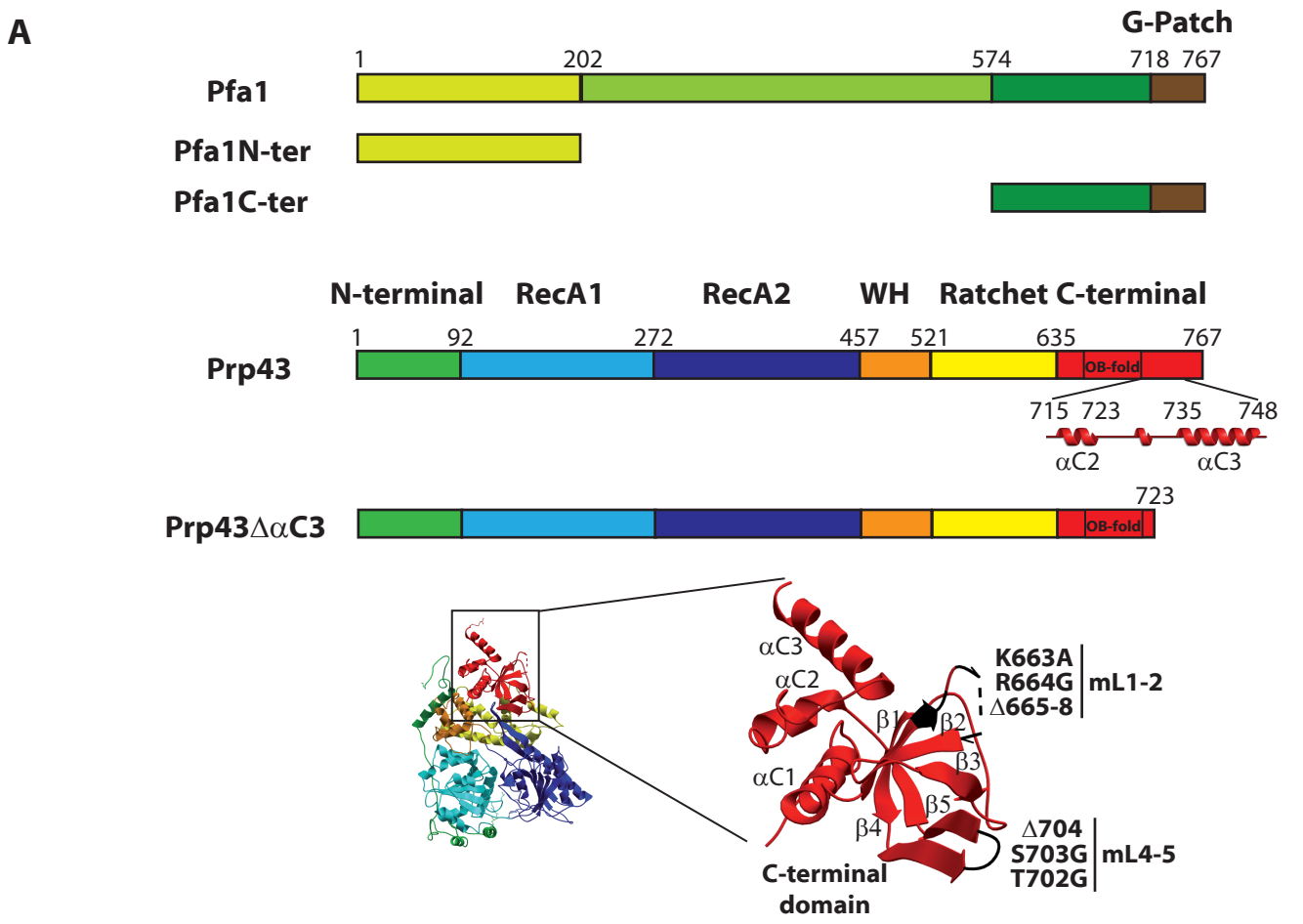
A
G-Patch
1
202
574
718
767
Pfa1
Pfa1N-ter
Pfa1C-ter
N-terminal
RecA1
RecA2
WH
Ratchet
C-terminal
1
92
272
457
521
635
767
Prp43
OB-fold
715
723
735
748
αC2
αC3
Prp43ΔαC3
723
OB-fold
αC3
αC2
αC1
β1
β2
β3
β4
β5
K663A
R664G
Δ665-8
mL1-2
Δ704
S703G
T702G
mL4-5
C-terminal domain

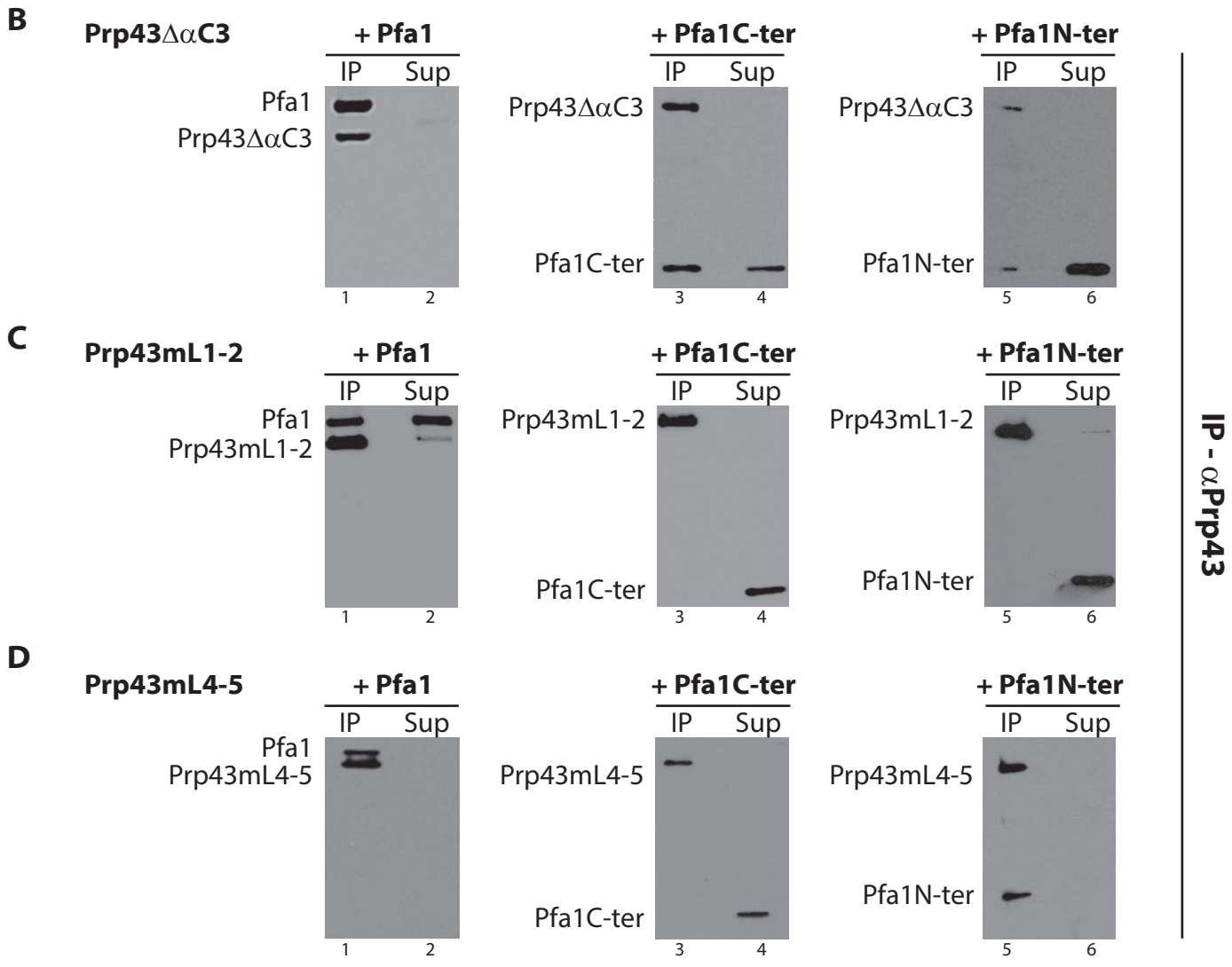
B
Prp43ΔαC3
+ Pfa1
IP
Sup
Pfa1
Prp43ΔαC3
1
2
+ Pfa1C-ter
IP
Sup
Prp43ΔαC3
Pfa1C-ter
3
4
+ Pfa1N-ter
IP
Sup
Prp43ΔαC3
Pfa1N-ter
5
6
C
Prp43mL1-2
+ Pfa1
IP
Sup
Pfa1
Prp43mL1-2
1
2
+ Pfa1C-ter
IP
Sup
Prp43mL1-2
Pfa1C-ter
3
4
+ Pfa1N-ter
IP
Sup
Prp43mL1-2
Pfa1N-ter
5
6
D
Prp43mL4-5
+ Pfa1
IP
Sup
Pfa1
Prp43mL4-5
1
2
+ Pfa1C-ter
IP
Sup
Prp43mL4-5
Pfa1C-ter
3
4
+ Pfa1N-ter
IP
Sup
Prp43mL4-5
Pfa1N-ter
5
6
IP - αPrp43

Figure 2

Figure 2

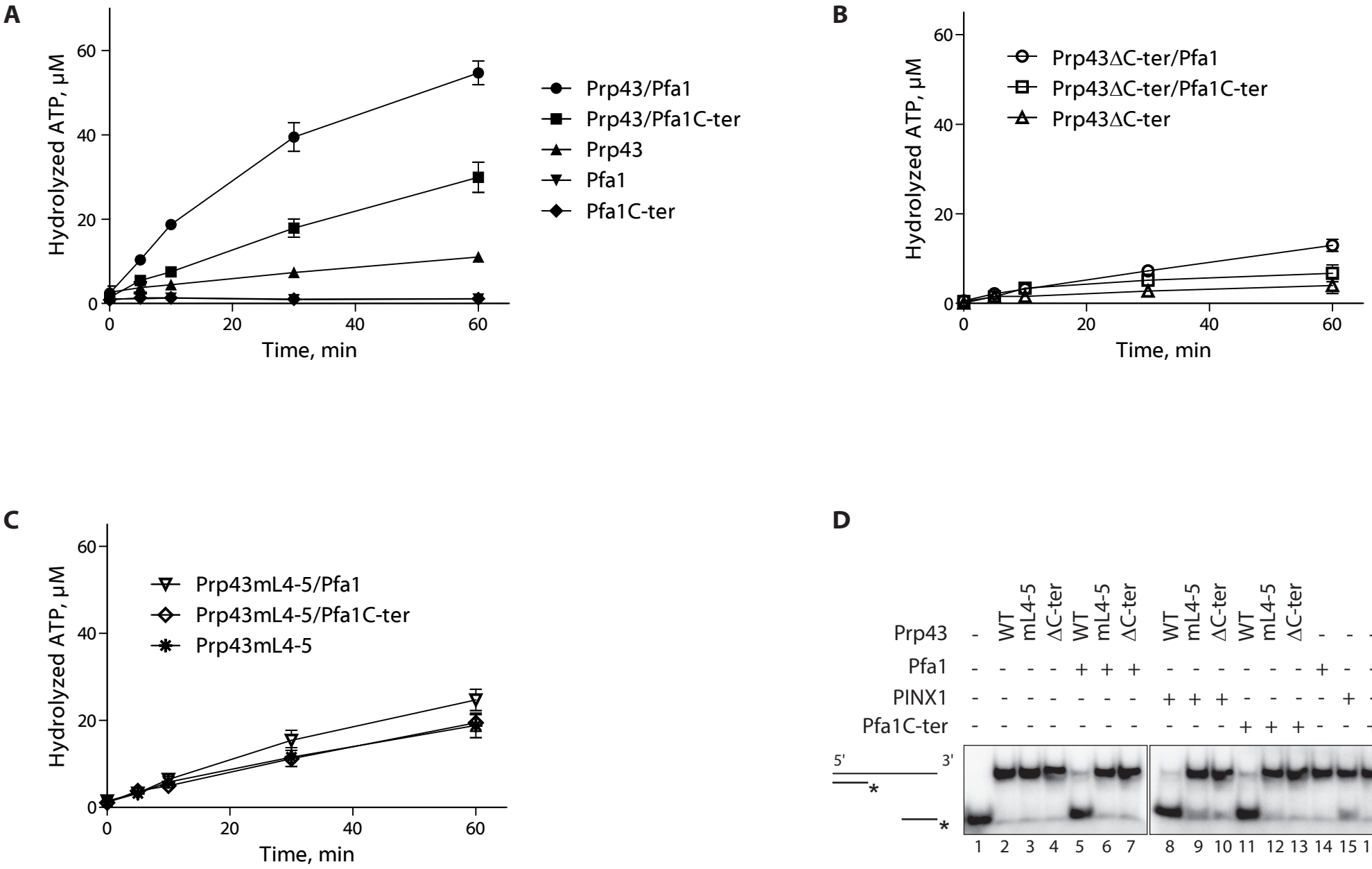

Figure 3

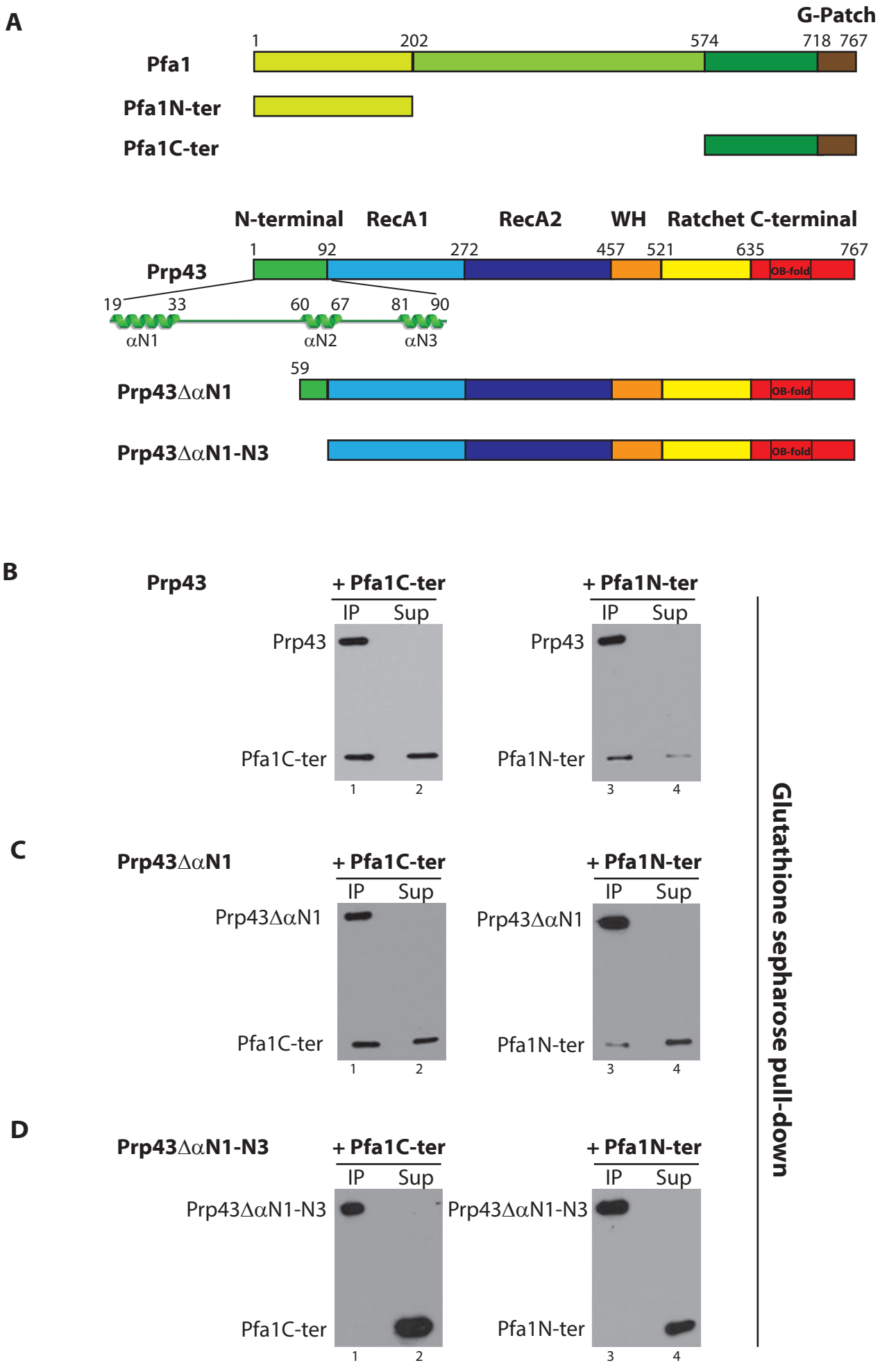
A
G-Patch
1
202
574
718 767
Pfa1
Pfa1N-ter
Pfa1C-ter
N-terminal
RecA1
RecA2
WH
Ratchet C-terminal
1
92
272
457
521
635
767
Prp43
OB-fold
19
33
60
67
81
90
αN1
αN2
αN3
59
Prp43ΔαN1
Prp43ΔαN1-N3
B
Prp43
+ Pfa1C-ter
+ Pfa1N-ter
IP
Sup
Prp43
Pfa1C-ter
Pfa1N-ter
1
2
3
4
C
Prp43ΔαN1
Prp43ΔαN1
D
Prp43ΔαN1-N3
Prp43ΔαN1-N3
Glutathione sepharose pull-down

Figure 4

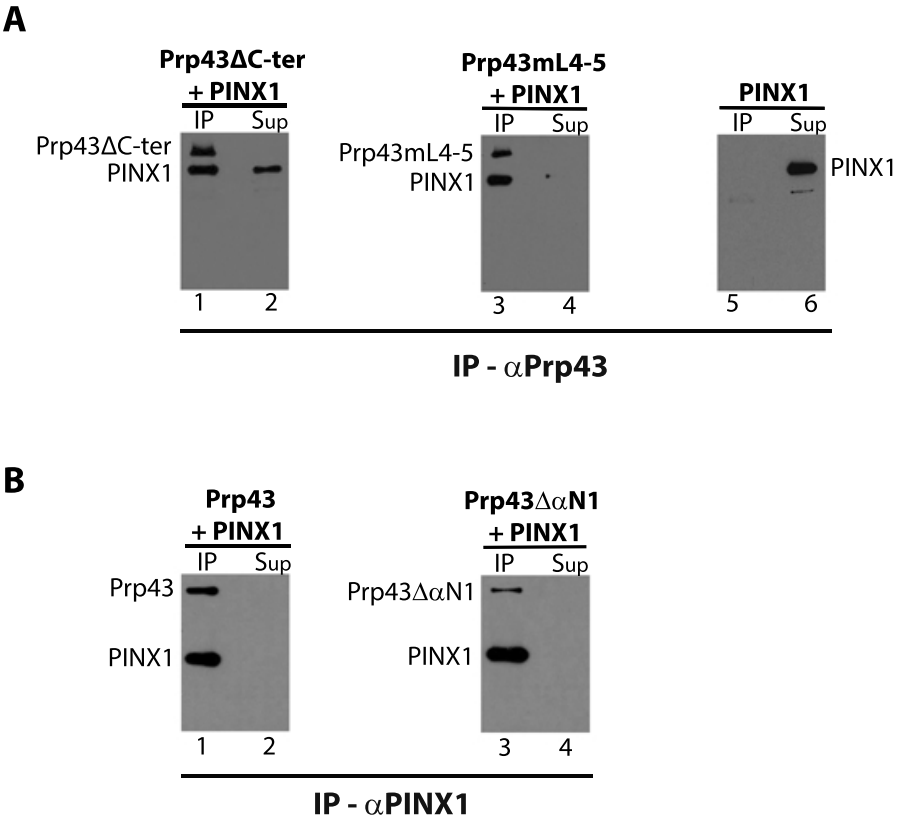
A
Prp43ΔC-ter
+ PINX1
IP
Sup
Prp43ΔC-ter
PINX1
1
2
Prp43mL4-5
+ PINX1
IP
Sup
Prp43mL4-5
PINX1
3
4
PINX1
IP
Sup
PINX1
5
6
IP - αPrp43
B
Prp43
+ PINX1
IP
Sup
Prp43
PINX1
1
2
Prp43ΔαN1
+ PINX1
IP
Sup
Prp43ΔαN1
PINX1
3
4
IP - αPINX1

Figure 5

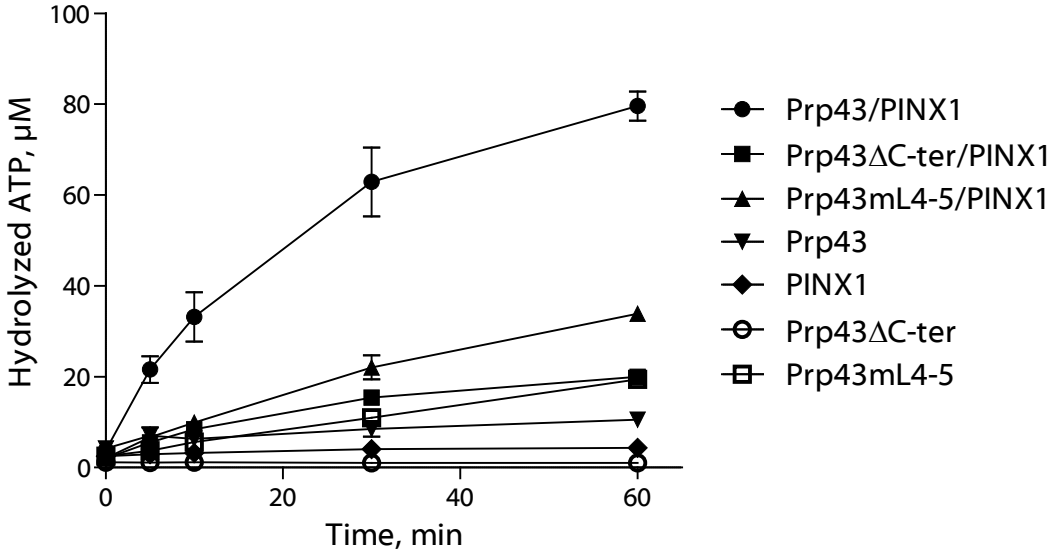
Hydrolyzed ATP, µM
100
80
60
40
20
0
0
20
40
60
Time, min
Prp43/PINX1
Prp43ΔC-ter/PINX1
Prp43mL4-5/PINX1
Prp43
PINX1
Prp43ΔC-ter
Prp43mL4-5

Figure 6

A

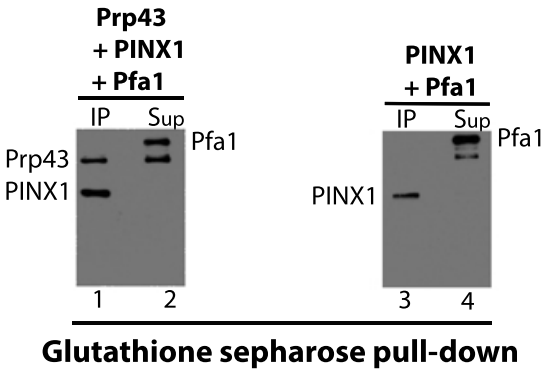
Prp43
+ PINX1
+ Pfa1
IP
Sup
Pfa1
Prp43
PINX1
1
2
PINX1
+ Pfa1
IP
Sup
Pfa1
PINX1
3
4
Glutathione sepharose pull-down

B

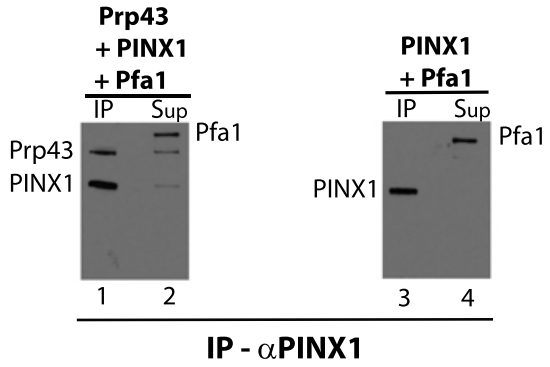
Prp43
+ PINX1
+ Pfa1
IP
Sup
Pfa1
Prp43
PINX1
1
2
PINX1
+ Pfa1
IP
Sup
Pfa1
PINX1
3
4
IP - αPINX1

Figure 7

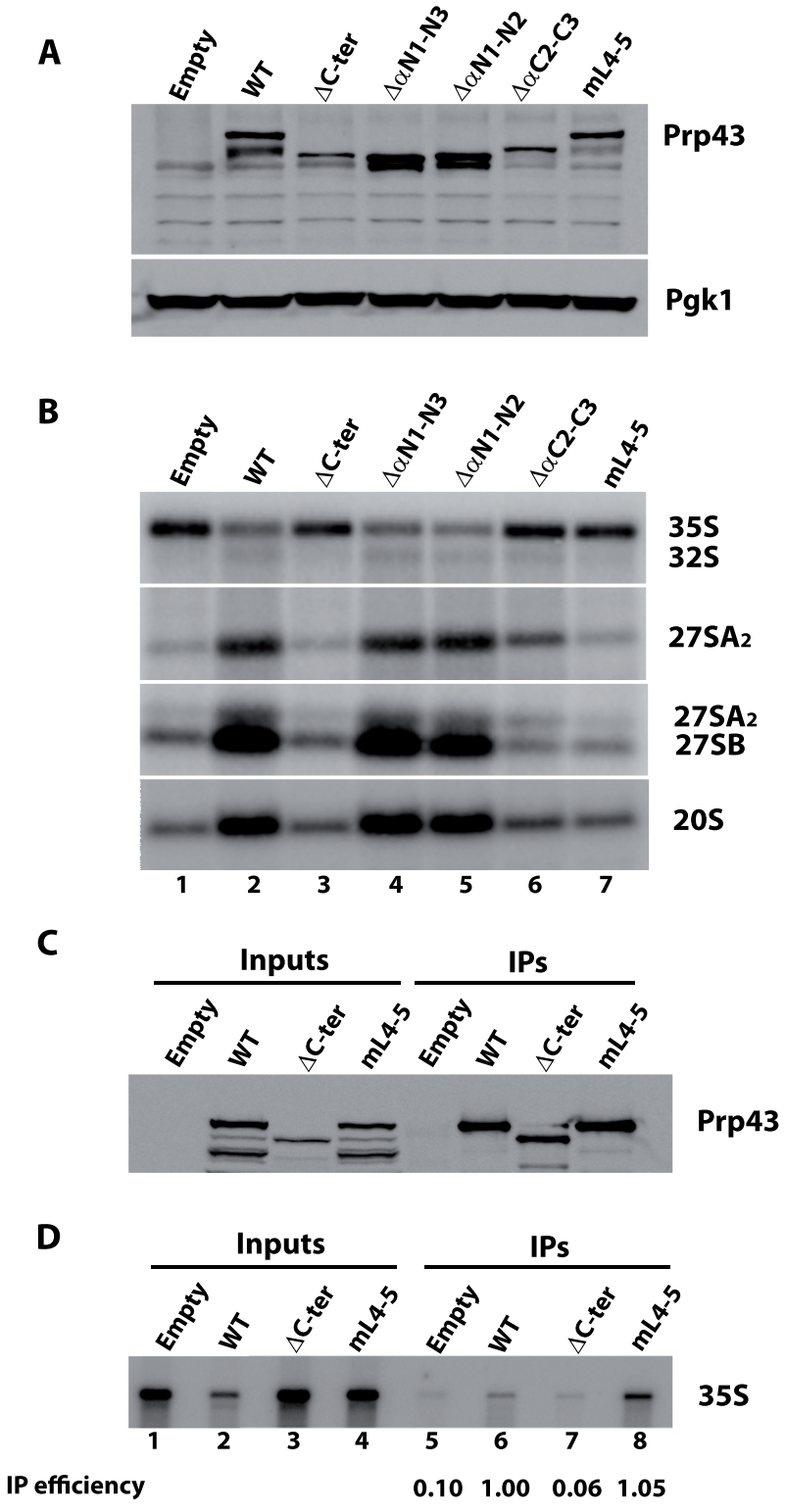
A
Empty
WT
ΔC-ter
ΔαN1-N3
ΔαN1-N2
ΔαC2-C3
mL4-5
Prp43
Pgk1
B
Empty
WT
ΔC-ter
ΔαN1-N3
ΔαN1-N2
ΔαC2-C3
mL4-5
35S
32S
27SA2
27SA2
27SB
20S
1 2 3 4 5 6 7
C
Inputs
IPs
Empty
WT
ΔC-ter
mL4-5
Empty
WT
ΔC-ter
mL4-5
Prp43
D
Inputs
IPs
Empty
WT
ΔC-ter
mL4-5
Empty
WT
ΔC-ter
mL4-5
35S
1 2 3 4 5 6 7 8
IP efficiency
0.10 1.00 0.06 1.05

Figure S1

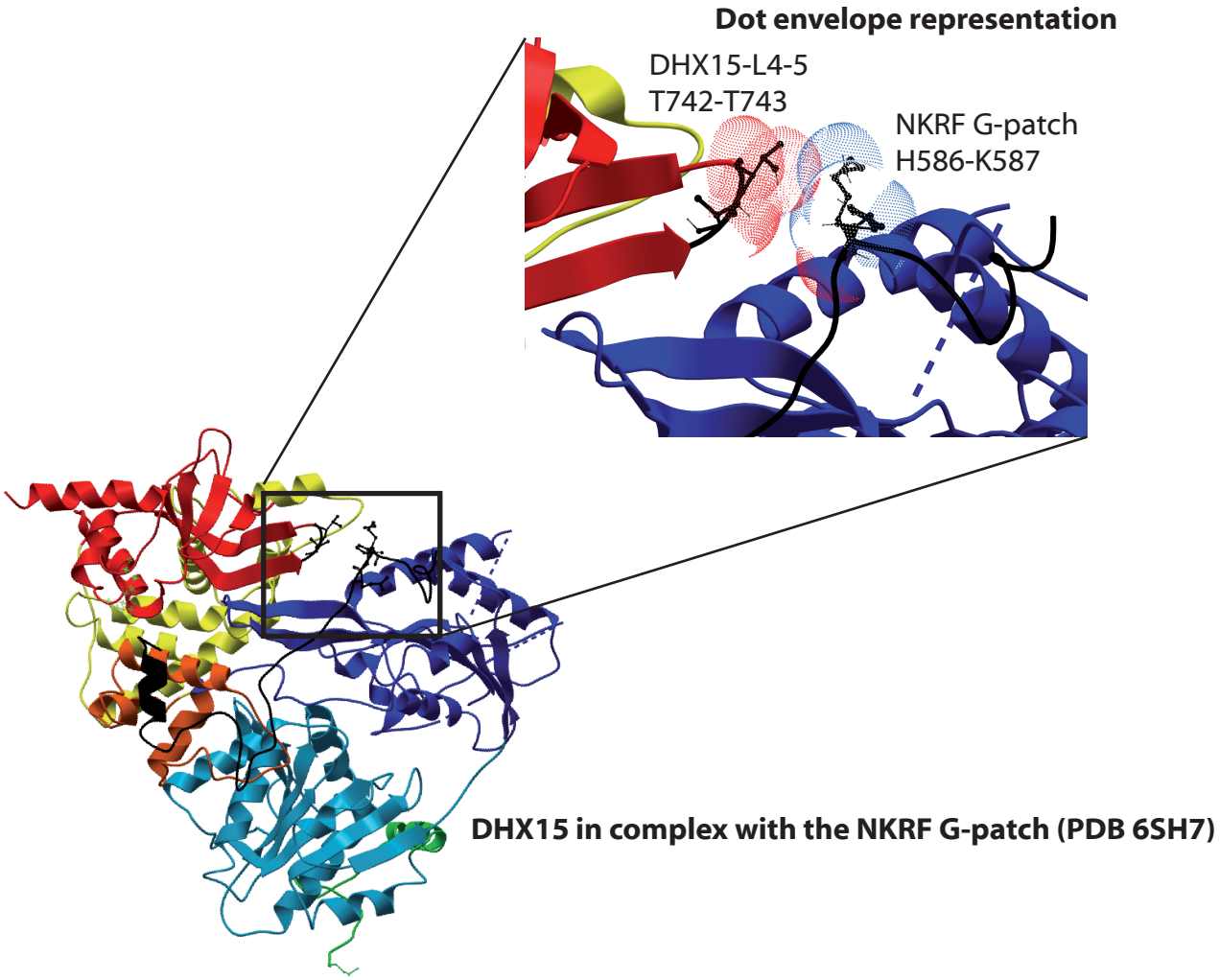
Dot envelope representation
DHX15-L4-5
T742-T743
NKRF G-patch
H586-K587
DHX15 in complex with the NKRF G-patch (PDB 6SH7)

Figure S2

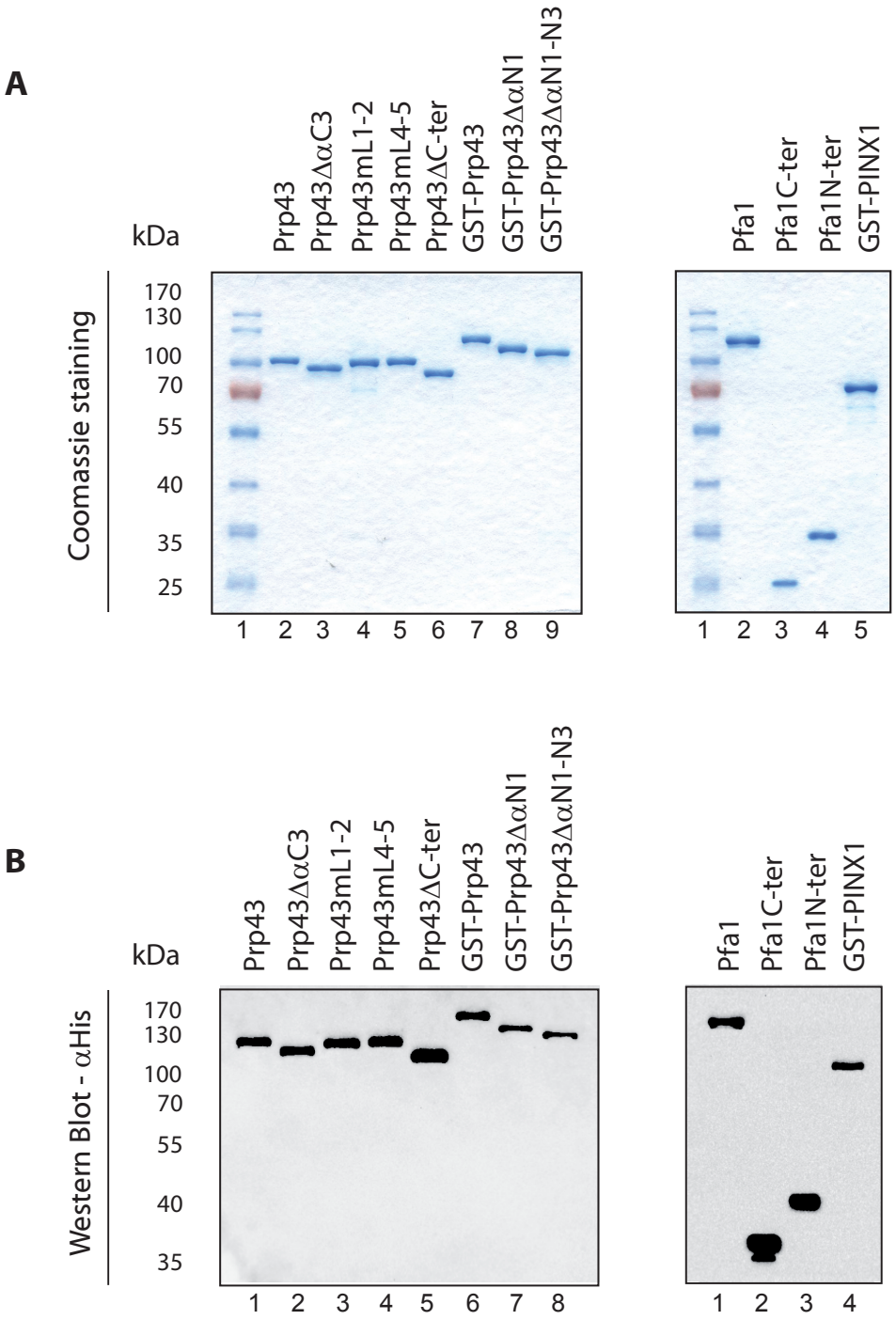
A
kDa
Coomassie staining
170
130
100
70
55
40
35
25
Prp43
Prp43ΔαC3
Prp43mL1-2
Prp43mL4-5
Prp43ΔC-ter
GST-Prp43
GST-Prp43ΔαN1
GST-Prp43ΔαN1-N3
1 2 3 4 5 6 7 8 9
Pfa1
Pfa1C-ter
Pfa1N-ter
GST-PINX1
1 2 3 4 5
B
kDa
Western Blot - αHis
170
130
100
70
55
40
35
Prp43
Prp43ΔαC3
Prp43mL1-2
Prp43mL4-5
Prp43ΔC-ter
GST-Prp43
GST-Prp43ΔαN1
GST-Prp43ΔαN1-N3
1 2 3 4 5 6 7 8
Pfa1
Pfa1C-ter
Pfa1N-ter
GST-PINX1
1 2 3 4

Figure S3

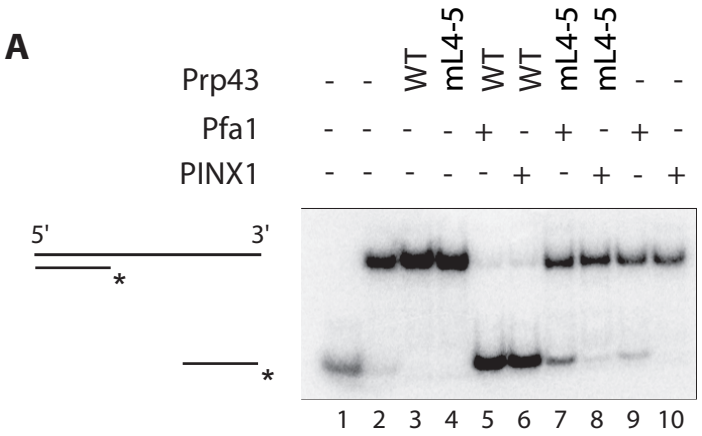
A
Prp43 - - WT mL4-5 WT WT mL4-5 mL4-5 - -
Pfa1 - - - - + - + - + -
PINX1 - - - - - + - + - +
5'
3'
*
*
1 2 3 4 5 6 7 8 9 10

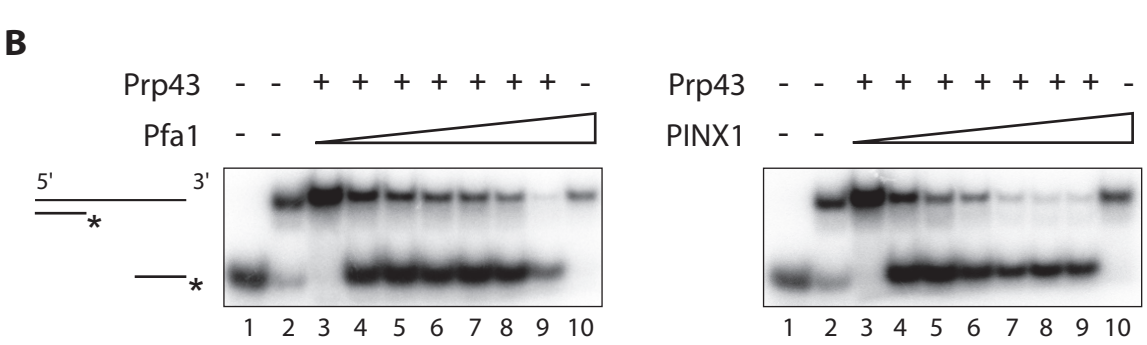
B
Prp43 - - + + + + + + + -
Pfa1 - -
5'
3'
*
*
1 2 3 4 5 6 7 8 9 10
Prp43 - - + + + + + + + -
PINX1 - -
1 2 3 4 5 6 7 8 9 10

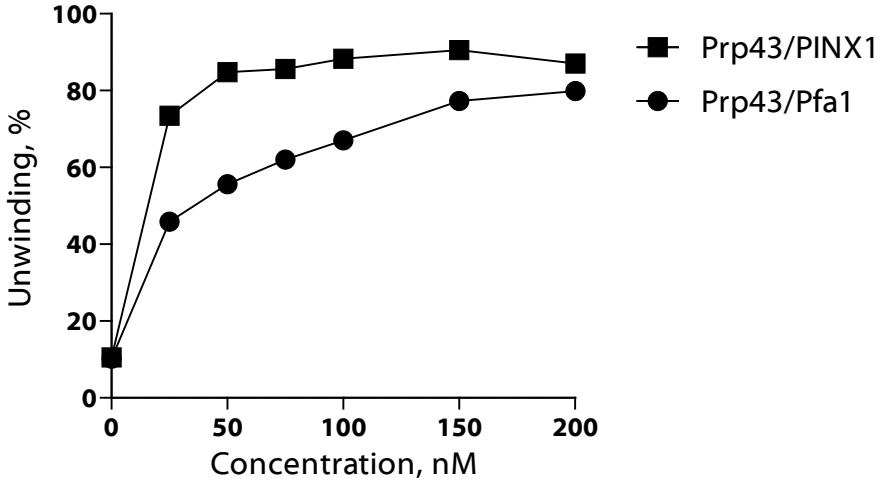
Unwinding, %
100
80
60
40
20
0
0 50 100 150 200
Concentration, nM
Prp43/PINX1
Prp43/Pfa1

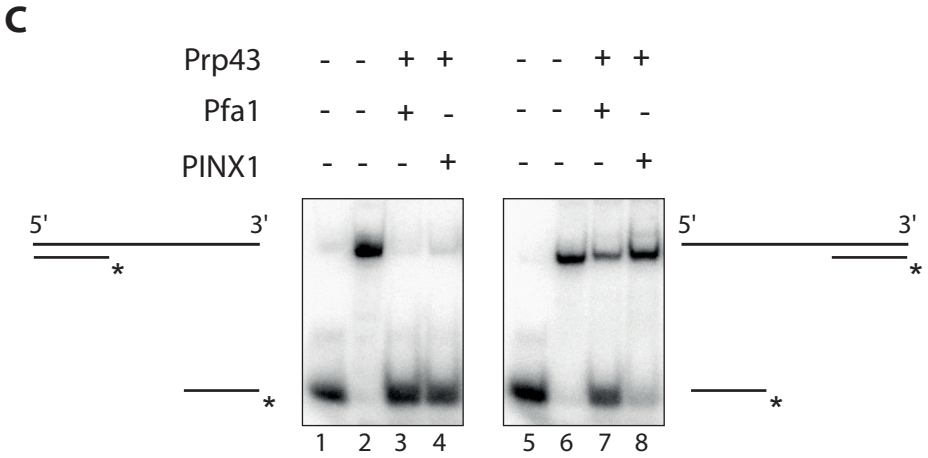
C
Prp43 - - + + - - + +
Pfa1 - - + - - - + -
PINX1 - - - + - - - +
5'
3'
*
*
1 2 3 4
5 6 7 8
5'
3'
*
*

Figure S4

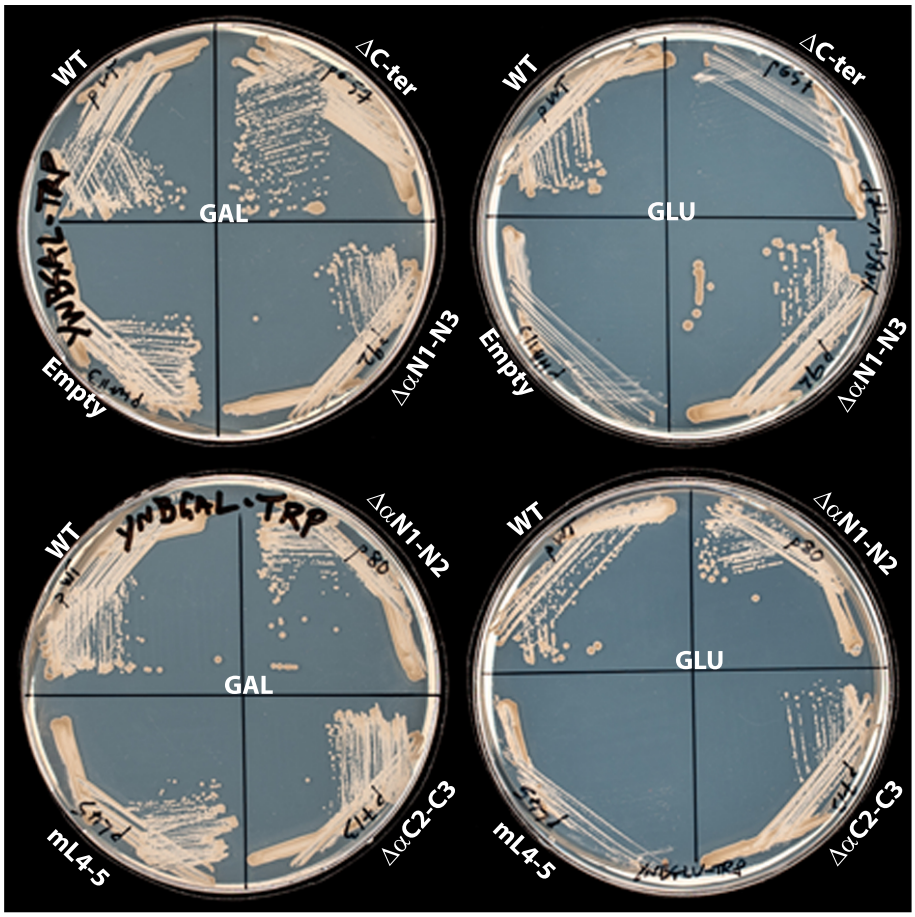
WT
ΔC-ter
GAL
Empty
ΔαN1-N3
WT
ΔC-ter
GLU
Empty
ΔαN1-N3
WT
ΔαN1-N2
GAL
mL4-5
ΔαC2-C3
WT
ΔαN1-N2
GLU
mL4-5
ΔαC2-C3

Figure S5

A

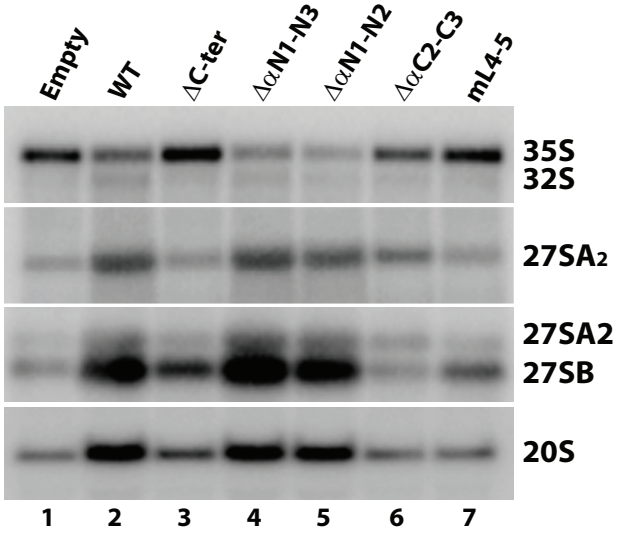
Empty
WT
ΔC-ter
ΔαN1-N3
ΔαN1-N2
ΔαC2-C3
mL4-5
35S
32S
27SA2
27SA2
27SB
20S
1
2
3
4
5
6
7

B

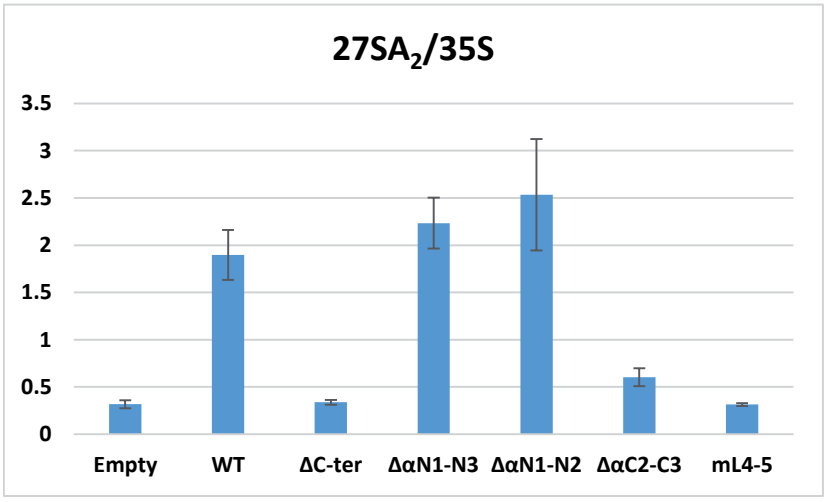
27SA2/35S
3.5
3
2.5
2
1.5
1
0.5
0
Empty
WT
ΔC-ter
ΔαN1-N3
ΔαN1-N2
ΔαC2-C3
mL4-5

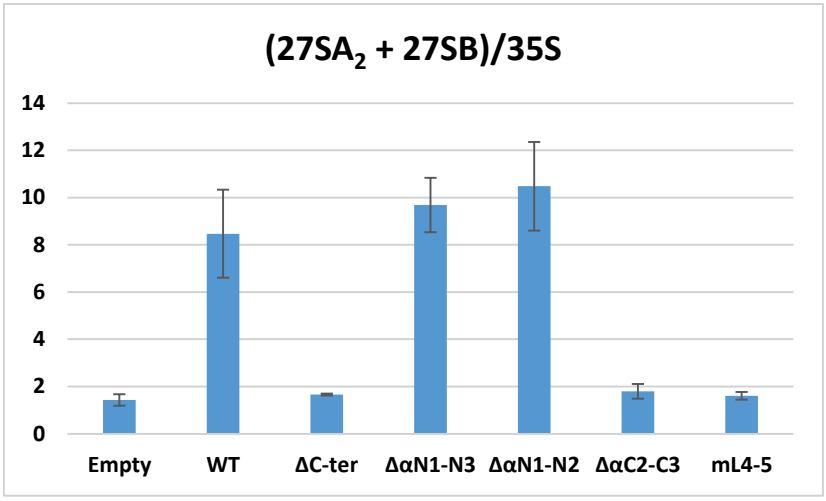
(27SA2 + 27SB)/35S
14
12
10
8
6
4
2
0
Empty
WT
ΔC-ter
ΔαN1-N3
ΔαN1-N2
ΔαC2-C3
mL4-5

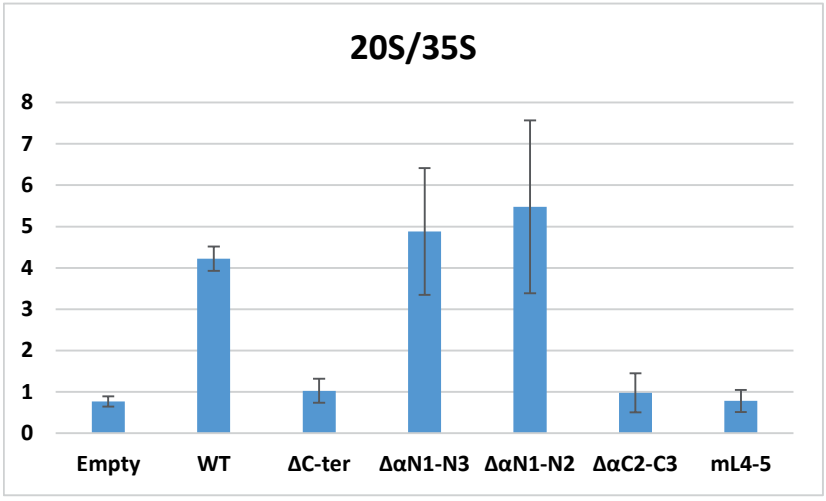
20S/35S
8
7
6
5
4
3
2
1
0
Empty
WT
ΔC-ter
ΔαN1-N3
ΔαN1-N2
ΔαC2-C3
mL4-5

Table S1

			G-patch proteins											
			Pfa1									PINX1		
			WT			C-ter			N-ter					
Prp43	**Growth**	**Pre-rRNA Processing**	**Interaction**	**ATPase activity**	**Helicase activity**	**Interaction**	**ATPase activity**	**Helicase activity**	**Interaction**	**ATPase activity**	**Helicase activity**	**Interaction**	**ATPase activity**	**Helicase activity**
WT	+	+	+	+	+	+	+	+	+	-	-	+	+	+
ΔC-ter	-	-	+	-	-	-	-	-	+			+	-	-
ΔαC3			+			+			+					
ΔαC2–C3	+/-	+/-												
mL1-2			+			-			-					
mL4-5	-	-	+	-	-	-	-	-	+			+	+/-	-
ΔαN1						+			+			+		

Table S2

Statistical analysis of rRNA processing intermediate ratios

Analysis of variances	27SA$_2$/35S		(27SA$_2$+27SB)/35S	20S/35S
Global analysis (all strains)				
F	20.9		25.16	7.75
p	$3.08\ 10^{-6}$		$9.8\ 10^{-7}$	$8.2\ 10^{-4}$
WT behavior (WT, ΔαN1-N3, ΔαN1-N2)				
F	0.93		0.62	0.3
p	0.44		0.57	0.75
Mutant behavior (Empty, ΔC-ter, ΔαC2-C3, mL4-5)				
F	0.29*	11.39**	0.75	0.32
p	0.76*	$2.9\ 10^{-3}$**	0.55	0.81
WT vs mutant behavior				
F	116.9		166.16	55.58
p	$1.47\ 10^{-9}$		$7.67\ 10^{-11}$	$4.7\ 10^{-7}$

F and *p*-values were computed with the Excel software for the cases indicated in the leftmost column, using the pre-rRNA ratios from three biological replicates of the Northern analysis.

* without taking into account the 27SA$_2$/35S ratio for the ΔαC2-C3 mutant.

** taking into account the 27SA$_2$/35S ratio for the ΔαC2-C3 mutant.

Dr Renee Schroeder
Editor-in-Chief
RNA Biology

Dear Dr Schroeder,

Please find below a point-by-point answer to the reviewers' comments. The corresponding changes to the manuscript text are highlighted in yellow.

To answer the concerns of the reviewers, we have added the following new figures and tables:

- Figure S1: Published NKRF G-patch/DHX15 complex with the position of the loop connecting the beta strands 4 and 5 highlighted.

- Figure S2: Coomassie-stained gel and Western analysis of all purified proteins used in pull-down/immunoprecipitation, ATPase and helicase assays.

- Figures S3: Helicase assays: A. Replicates of the helicase assays shown in Figure 2D. B and C: panels A and B of former Figure S1.

- Figure S4: Former Figure S2.

- Figure S5: Replicate of Northern of Figure 7B and quantitative analysis of pre-rRNA processing differences.

- Table S1: Summary of the properties of Prp43 and G-patch proteins and their derivatives used in this work.

- Table S2: Statistical analysis of rRNA processing intermediate ratios.

Novel data have also been added to Figures 2, 5 and 7 as detailed below.

We hope that the manuscript will now be judged suitable for publication in *RNA Biology*.

Sincerely,

Yves Henry and Odile Humbert

Reviewer 1:

However, the authors should also include biological replicates of their data as appropriate. While the authors fulfill the one-replicate standard-of-proof common in the field for immunoprecipitation experiments, the rigor of this manuscript would be greatly strengthened by showing additional biological replicates for the ATPase, helicase, and pre-rRNA processing assays. Additionally, quantification of the pre-rRNA processing intermediate ratios and of the pulldown ratio in Figure 7D would further bolster the manuscript's conclusions.

Major comments:

1. *The authors should include biological replicates of the ATPase (Figure 2A-C, Figure 5), helicase assays (Figure 2D), or pre-rRNA processing northerns (Figure 7B).*

The standard errors of the mean (sem) based on three replicates are now indicated on the ATPase assay plots (Figure 2A-C, Figure 5). Helicase assays have been performed with additional mutants, namely Prp43 mutant Prp43ΔC-ter and Pfa1 mutant Pfa1C-ter (new Figure 2D). Additional helicase assays are presented in new Figure S3A. Replicates of pre-rRNA processing Northerns are presented in new Figure S5, quantifications of various pre-rRNA ratios have been performed and subjected to ANOVA statistical tests (see below, Figure S5 and Table S2).

2. *Figure 7B: To quantitatively communicate defects observed in pre-rRNA processing, the authors should graph the northern blot pre-rRNA processing results using Ratio Analysis of Multiple Precursor (RAMP) quantification for all replicates [Wang, M., Anikin, L. & Pestov, D.G. Two orthogonal cleavages separate subunit RNAs in mouse ribosome biogenesis. Nucleic Acids Res 42, 11180-11191 (2014)]. Appropriate ANOVA testing can then be used to illustrate statistically-significant differences in processing intermediate levels.*

We have performed ratio analyses taking into account the major pre-rRNA intermediates (35S, 27SA2, 27SB, 20S pre-rRNAs) using the Northern data from three biological replicates (new Figure S5). ANOVA has been performed with these ratios (Table S2), which indicates strongly statistically significant differences between the wild-type control and a subset of mutants.

3. *Figure 7D: The authors should quantify the pulldown ratio to clarify the result. It is difficult to compare WT and mL4-5 by eye because of unequal loading.*

The immunoprecipitation efficiency of 35S pre-rRNA in mutants relative to wild-type has been quantified and is now indicated below each IP lane (Figure 7D).

Minor comments:

4. *Figure 2D: Correct PINXI to PINX1.*

This has been corrected throughout.

5. *p. 6: I don't think [30] contains the cited Pfa1N-ter and Prp43ΔC-ter experiment. However, this is shown in [17] (Figure 6, lane 11). The citation should be corrected.*

This citation has been corrected.

6. *p. 11: Correct phrasing in sentence "In contrast, cells expressing Prp43ΔN1-N2 or Prp43ΔN1-N3 grow in glucose-containing medium as cells expressing wild-type Prp43." to "grow in glucose-containing medium as well as cells expressing wild-type Prp43."*

This sentence has been corrected.

7. *All immunoprecipitation figures: I recommend noting which antibody was used for pulldown in each immunoprecipitation figure panel. The antibodies used in Figure 6 were not obvious, although they are in the legend. It would make the story easier to follow.*

The antibodies or type of sepharose used have been indicated in each immunoprecipitation/pull-down figure panel.

Reviewer 2:

1. *While an assay of the ATPase activity is a useful start, it would be equally useful to assess helicase activity, at least with a subset of the most important mutants.*

As indicated above in the answer to point 1 of reviewer 1, helicase assays have been performed with additional mutants, namely Prp43 mutant Prp43ΔC-ter and Pfa1 mutant Pfa1C-ter (new Figure 2D).

2. *The inputs of the in vitro pulldowns must be shown in order to assess them properly. Without those one cannot draw any strong conclusions from the pulldowns.*

All our pull-down/immunoprecipitation experiments have been performed with the same amounts of purified recombinant proteins, not with cell extracts. Moreover, we have shown the unbound material (supernatant) for each pull-down/immunoprecipitation, hence from the data presented it is clear what proportion of input protein is precipitated. We have now included a Coomassie stained gel of all the purified proteins used and a corresponding Western blot (new Figure S2).

3. *Full length Pfa1 and PINX1 both bind to Prp43mL4-5. It is only when they use the two Pfa1 fragments that deficiencies in binding to Prp43mL4-5 are uncovered. A similar experiment with PINX1 was not done. Thus, the conclusion that Pfa1 and PINX1 interact with Prp43 differently is not supported by the data. The authors should compare the binding of the G patch domain of Pfa1 with the G patch domain of PINX1 on binding of Prp43ΔC-ter or Prp43mL4-5.*

Our previously published data indicate that Pfa1 deleted of its G patch can still interact with Prp43. In sharp contrast, point mutations within the G patch of full length PINX1 prevent its binding to full length Prp43 both *in vitro* and in yeast cells (Chen et al., Nucleic Acids Res., 2014). Hence, contrary to Pfa1 G patch, the G patch of PINX1 is essential for its binding to Prp43. Thus our finding that PINX1 interacts with Prp43ΔC-ter or Prp43mL4-5 indicates that its G-patch does not require Prp43 C-terminal domain for binding.

4. *I am assuming that the authors were trying to make a mutant that separates the Gno1 and Pfa1-dependent functions of Prp43. While they found a mutant that is deficient only in Pfa1 binding, this mutant turned out to be useless because it is required for Gno1/PINX1-dependent Prp43 activation. Why did the authors not carry out a more comprehensive analysis of Prp43 truncations and mutants for some deficient in Gno1/PINX1 binding? At the very least, one would expect them to test all the ones tested for Pfa1. But to be honest, in order for this to be a meaningful contribution for the field, I think one should have a separation mutant.*

While we agree with the reviewer that obtaining a separation mutant would have been very interesting, we do think that providing evidence for the crucial role of the OB fold domain and in particular its beta 4- beta 5 loop is an important contribution to the field.

5. *The manuscript is extremely hard to follow. I would suggest the authors lead with a Figure of the published G-patch/DEAH-helicase complex, to better illustrate the rationale for these experiments. A summary of the roles of the different elements in Prp43, PINX1 and Pfa1 studied in here for binding and activation by the G-patch proteins would also be helpful.*

We have included a figure of the published NKRF G-patch/DHX15 complex and highlighted the position of the loop connecting the beta strands 4 and 5 (new Figure S1). We also added a table (Table S1) summarising the roles of the domains of Prp43 and G-patch proteins studied here.